SEMARAK ILMU PUBLISHING

Journal of Advanced Research in Fluid Mechanics and Thermal Sciences

Journal homepage:
https://semarakilmu.com.my/journals/index.php/fluid_mechanics_thermal_sciences/index
ISSN: 2289-7879

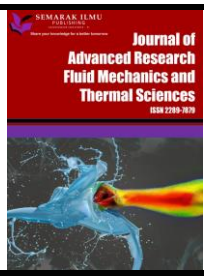

Numerical Simulation of the Tree Effects on Wind Comfort and Wind Safety Around Coastline Building Resort

Husna Aini Swarno[1], Nurul Huda Ahmad[1,*], Ahmad Faiz Mohammad[2], Nurnida Elmira Othman[3]

[1] Razak Faculty of Technology and Informatics (RFTI), Universiti Teknologi Malaysia Kuala Lumpur, Jalan Sultan Yahya Petra, 54100 Kuala Lumpur, Malaysia
[2] Malaysia-Japan International Institute of Technology (MJIIT), Universiti Teknologi Malaysia Kuala Lumpur, Jalan Sultan Yahya Petra, 54100 Kuala Lumpur, Malaysia
[3] School of Mechanical Engineering, College of Engineering, Universiti Teknologi Mara (UiTM), 40450 Shah Alam, Selangor, Malaysia

ARTICLE INFO

Article history:
Received 5 November 2023
Received in revised form 1 April 2024
Accepted 16 April 2024
Available online 15 May 2024

Keywords:
Strong wind; coastal; windbreak; Casuarina equisetifolia; wind comfort

ABSTRACT

Beach resorts located in coastal areas are particularly vulnerable to natural disasters and extreme weather events. Climate change exacerbates these risks, with rising sea levels, intense rainfall, and cyclones impacting coastal communities, including hotel operators. This study aims to address the challenge of tropical storms resulting from climate change in Langkawi's coastline region, specifically focusing on mitigating their impact on pedestrian wind comfort. The research investigates the quantitative impact of vegetative windbreaks on wind velocity at an open-building resort in Cenang, Langkawi, Malaysia. The goal is to propose effective strategies for reducing wind velocity and enhancing pedestrian wind comfort for beachfront resorts. The primary objective is to determine the optimal arrangement of vegetative windbreaks that provide optimal wind comfort for buildings. Numerical simulations were conducted to analyze flow characteristics around tree windbreaks, with validation through wind tunnel experiments. The simulation method, employing the RNG k-ε turbulence closure scheme, accurately predicted airflow patterns for both single and double rows of trees, treating the trees as porous media with defined aerodynamic properties. Results indicate that staggered double rows of windbreaks offer the most significant improvement in wind shelter, with a maximum mean Boundary Effectiveness Index (mBEI) of approximately 1.92. This configuration ensures greater downwind shelter distances compared to linear double rows and single-row windbreaks, thus enhancing wind comfort. Enhanced wind comfort is crucial for promoting safety and enjoyment during outdoor activities at resort facilities. Strategically planting windbreak trees enables resort management to create a more pleasant environment for guests, shielding them from strong winds while preserving aesthetic appeal. This study offers practical guidelines for resort developers, emphasizing optimal row arrangements and windbreak designs that balance environmental aesthetics with pedestrian wind comfort. Implementing these practices enhances the overall experience for resort guests, contributing to a safer and more enjoyable leisure environment.

* *Corresponding author.*
E-mail address: nurulhuda.kl@utm.my

https://doi.org/10.37934/arfmts.117.1.142

1. Introduction

The tourism industry has played a major role in driving Malaysia's economic growth, serving as a critical component in the country's overall economic development strategy. Malaysia's tourism industry experienced a period of consistent growth in the four years from 2015 to 2019, with the number of tourist arrivals increasing from 25.72 million in 2015 to 26.10 million in 2019. This remarkable growth has propelled the tourism sector to the forefront of countries' economic expansion [1].

Beach resorts are common destinations for both local and foreign tourists in Malaysia. Mustapha and Awang [2] reported a steady increase in the number of beach resorts, particularly those located on islands, resulting in fierce competition among them. However, during the monsoon season from November to March, beach resorts on the east coast of Malaysia face significant challenges due to heavy rain and rough seas, which force them to temporarily close their businesses. As a result, there is a substantial decrease in the number of tourists visiting the islands during this period. Despite these challenges, beach resorts continue to attract a significant number of tourists throughout the year, due to scenic beaches and various attractions [3].

The development of beach resorts in the Asia Pacific region often begins positively but ultimately results in negative features and impacts, including a decline in quality over time, increased congestion and pollution, and a reduction in the quality of beach-related recreation [4]. These negative impacts have consequences for the hotel industry, with hotel management facing challenges due to unpredictable weather and climate change, which can affect tourists' decisions to travel and stay at hotels. The impact of climate change is also adversely affecting coastal communities, including hoteliers, as rising sea levels, heavy rainfall, and cyclones could damage their property and hotel infrastructure [5].

As infrastructures such as road networks and commercial properties are developed to meet the growing demand in the tourism sector, the expansion of the built environment has led to uncontrolled urbanization around and near tourist sites [6]. However, the rapid and unplanned development and land clearing have resulted in various environmental impacts, including deforestation and the fragmentation of the island's forests, which threaten biodiversity. In addition, the development of coastal areas for beach accommodations has led to land reclamation, water pollution, and soil erosion [7].

Land reclamation activities that are not properly planned can cause adverse impacts on the coastline. High demand for stable land in coastal areas with the current modern technology, has increased the amount of coastal reclamation development, particularly for the construction of luxury building resorts adjacent to the beach. For instance, the coastline area along Kuah, Langkawi has undergone sea reclamation, and a mega development project involved 2,000 acres of reclaimed land under Widad Langkasuka in the coastal sea area near Padang Mat Sirat, Langkawi [8]. The large scale of coastal development not only poses serious impacts on the marine environment but adversely affects the local community, sea levels, and climate [9].

According to the National Property Information Centre report in the fourth quarter of 2022, there were 534 beach hotels in Malaysia, with the most significant numbers in Terengganu (136), Pahang (84), and Kedah (70) [10]. Moreover, Kedah has the highest number of five-star hotels with 10 hotels, followed by Pahang and Terengganu with 6 and 4 hotels respectively. Most of these luxury beach hotels are in Langkawi, Kedah, which was declared a Tourism City by the Malaysian government in 2000. Langkawi is well known for its pristine beaches, scenic beauty, richness of cultural heritage, and preserved tropical environments, making it one of the most popular tourist destinations in the country [11].

The construction of high-end or luxury beach resorts in Langkawi has been focused on various coastal locations, including Cenang Beach, Datai Bay, Tengah Beach, Tanjung Rhu Beach, Kok Beach, and Burau Bay, Kuah, and hilly rural settings in the central part of the island. Among these locations, Cenang Beach stands out as the most preferred spot for resort hotels [11]. The area hosts over 50 hotels, 45 restaurants, 125 retail shops, and 38 various service and entertainment providers, reflecting the high concentration of tourism-related products in the area due to high tourist arrivals and residency [12]. However, tourism development in Cenang Beach can cause overcrowding, traffic congestion, environmental degradation, and increased infrastructure and property costs. Most land grabs for construction in the coastal area particularly those adjacent to the beach, also disrupt ecological systems, affecting the stability of the island's ecosystem [13].

The negative effects of natural disasters and severe weather conditions have been observed on multiple occasions in Langkawi. Examples of these incidents include strong winds, heavy rainfall, and thunderstorms that have uprooted trees and knocked down power poles, as well as the damage caused by Tropical Storm Pabuk in late 2018 and Typhoon Lekima in 2019 [14,15]. More recently, a storm in November 2020 caused the roofs of houses and residential buildings in Kampung Yooi, Langkawi, to be ripped off, causing inconvenience to both residents and tourists [16]. These events have been linked to the impact of the land reclamation development and caused inconvenience to the residents and foreign tourists. Despite these challenges, the recognition of Langkawi as a global geopark by UNESCO in 2007 has spurred Langkawi Development Authority to promote sustainable development in the area.

Therefore, further research is needed in numerical analysis to investigate and analyze the flow characteristics of the open resort building when Langkawi is hit by storms and strong winds. This can be achieved by planting single or multiple rows of trees or shrubs as living windbreaks to reduce the impact of strong winds near the coastline. Windbreaks or shelterbelts are effective barriers that reduce wind velocity and alter wind fields [17,18]. Windbreaks work by building up the pressure at the windward side as the wind blows against them, causing large quantities of air to move up and over the top or around the ends of the windbreaks. Living windbreaks consist of plantings of single or multiple rows of trees, as well as fences or other materials. The reduction in wind velocity behind a windbreak modifies the environmental conditions or microclimate in the sheltered zone [19].

To ensure accuracy in the simulation study, significant values such as the drag coefficient of the tree need to be precisely determined [20]. The effectiveness of Computational Fluid Dynamics (CFD) in simulating flow around tree windbreaks has been proven through numerical simulations, allowing for quantitative visualization and investigation of velocity reduction [21]. This study focused on evaluating the suitability of windbreaks, specifically for the common vegetative windbreaks in Langkawi such as Cenang Beach and many other beach resorts found in Malaysia. The simulation conducted in this study aimed to assess the effectiveness of windbreaks in reducing the impact of strong winds on the open building resort located near coastal areas.

In summary, it can be observed that land reclamation development in Langkawi has resulted in the occurrence of storms, strong winds, and heavy rainfall, likely due to climate alteration in the coastal region. To minimize the impact of future tropical storms, further numerical investigations are necessary to determine effective ways to reduce strong winds along the coastline. The use of vegetation such as shrubs or trees as windbreaks has been recognized worldwide for its ability to reduce wind velocity and provide various benefits [22]. Therefore, incorporating vegetation as a windbreak in Langkawi may prove to be an effective solution in mitigating the impact of tropical storms in the area.

1.1 Site Description

Langkawi was selected as the site location because of its increasing number of tourists and its large urban development area of approximately 36,342 hectares. According to the Langkawi Municipal Council [13], the island has a hilly topography and is surrounded by a forest reserve, which has an area of about 26,266 ha and covers 54.6% of the total land area. Cenang was the focus of this study as it is the main tourist area on the island and many development projects are still ongoing in this area. Cenang beach, which is well-equipped and has several beach resorts, is the most popular tourist attraction [23]. The Holiday Villa Beach Resort was chosen because of the topography and location of its three-story building, which was ideal for this study. Figure 1 shows the layout of the resort, which is situated at Jalan Pantai Cenang, Langkawi.

(a) (b)

Fig. 1. The site location at Jalan Pantai Cenang, Langkawi: (a) top view, and (b) side view. The yellow dashed box in (a) denotes the Holiday Villa Beach Resort [24,25]

The resort is surrounded by coconut and Syzygium Grande (SG) trees. Under strong wind conditions, the coconuts might fall from the trees, and this can be dangerous to pedestrians. According to Foale [26], the weight of a mature coconut varies from 0.6 to 3.0 kg, depending on the type of palm. Therefore, pedestrians should be notified of the danger of falling coconuts near the resort to prevent any injuries or unwanted incidents. SG trees can be found throughout the tropical Asian region in a large variety of habitats [27]. These include coastal forests, which can be commonly found in Singapore. The common names of the SG tree include Sea Apple and Jambu Laut or Jambu Air Laut [28]. It is capable of growing up to 30 m in canopy height [29]. However, this tree does not tolerate strong wind and waterlogged conditions because of its fragile wood, as reported by Whistler and Elevitch [30].

2. Methodology

2.1 Numerical Model

CFD simulations were conducted based on RANS equations and assumes a three-dimensional, non-rotating, non-hydrostatic, incompressible airflow system was considered. The turbulence was parameterized using the renormalization group (RNG) *k-ε* turbulence closure scheme [31]. To account for the airflow pressure loss caused by trees, the tree drags terms added to the equations of momentum, the turbulent kinetic energy (k), and turbulent kinetic energy dissipation rates (ε), as in Ries and Eichhorn [32] and Balczó *et al.,* [33]. RANS for momentum and mass conservation can be expressed as follows [34]

$$\frac{\partial U_i}{\partial t} + U_j \frac{\partial U_i}{\partial x_j} = -\frac{1}{\rho}\frac{\partial P^*}{\partial x_i} + v\frac{\partial^2 U_i}{\partial x_i x_j} - \frac{\partial}{\partial x_j}\left(u_i u_j\right) + \frac{1}{\rho}F_{tree,i} \quad (1)$$

$$\frac{\partial U_j}{\partial x_j} = 0 \tag{2}$$

where x_i is the i^{th} cartesian coordinate (i = 1, 2, 3), U_i is the i^{th} mean velocity component, and P^* is the deviation of pressure from the reference value. For ρ and v are, the air density and kinematic viscosity respectively, whereas u_i is the fluctuation from the i^{th} mean velocity component. Reynolds stresses in Eq. (1) were parameterized as follows [34]

$$-u_i u_j = K_m \left(\frac{\partial U_i}{\partial x_j} + \frac{\partial U_j}{\partial x_i}\right) - \frac{2}{3}\delta_{ij} k \tag{3}$$

where K_m, k, and δ_{ij} are the turbulent diffusivity of momentum, turbulent kinetic energy, and the Kronecker delta respectively. The turbulent diffusivity of momentum was determined using k and ε as follows [34]

$$K_m = C_\mu \frac{k^2}{\varepsilon} \tag{4}$$

where C_μ = 0.0845 is an empirical constant of the RNG k-ε turbulence closure scheme. The prognostic equations of k and ε in the RNG k-ε turbulence closure scheme was written as follows [34]

$$\frac{\partial k}{\partial t} + U_j \frac{\partial k}{\partial x_j} = -u_i u_j \frac{\partial U_i}{\partial x_j} + \frac{\partial}{\partial x_j}\left(\frac{K_m}{\sigma_k}\frac{\partial k}{\partial x_j}\right) - \varepsilon + F_{tree,k} \tag{5}$$

$$\frac{\partial \varepsilon}{\partial t} + U_j \frac{\partial \varepsilon}{\partial x_j} = -C_{\varepsilon 1}\frac{\varepsilon}{k} u_i u_j \frac{\partial U_i}{\partial x_j} + \frac{\partial}{\partial x_j}\left(\frac{K_m}{\sigma_\varepsilon}\frac{\partial k}{\partial x_j}\right) - C_{\varepsilon 2}\frac{\varepsilon^2}{k} - R_s + F_{tree,\varepsilon} \tag{6}$$

where R_s is a strain rate term given as

$$R_s = \frac{C_\mu \gamma^3 (1-\frac{\gamma}{\gamma_0})\varepsilon^2}{(1+\beta_0\gamma^3)k} \tag{7}$$

$$\gamma = \frac{k}{\varepsilon}\left[\left(\frac{\partial U_i}{\partial x_j} + \frac{\partial U_j}{\partial x_i}\right)\frac{\partial U_i}{\partial x_j}\right]^{1/2} \tag{8}$$

where $C_{\varepsilon 1}$, $C_{\varepsilon 2}$, σ_k, σ_ε , γ_0 and β_0 are empirical constants specified as follows [34]

($C_{\varepsilon 1}$, $C_{\varepsilon 2}$, σ_k, σ_ε , γ_0, β_0) = (1.42, 1.68, 0.7179, 0.7179, 4.377, 0.012) (9)

The tree drag was represented by the sink and the source terms on the right-hand side of Eq. (1), Eq. (5), and Eq. (6) were expressed as follows [35,36]

$$F_{tree,i} = -\rho . {n_c}^3 . C_d . LAD . U_i . |U| \tag{10}$$

$$F_{tree,k} = {n_c}^3 . C_d . LAD . |u^3| - 4{n_c}^3 . C_d . k . |U| \tag{11}$$

$$F_{tree,\varepsilon} = \frac{3}{2}\frac{\varepsilon}{k} . {n_c}^3 . C_d . LAD . |u^3| - 6{n_c}^3 . C_d . \varepsilon . |U| \tag{12}$$

where n_c is the fraction of the area covered by the vertical projection of leaves (set to 1) and C_d is the leaf drag coefficient. The leaf area density (LAD) is defined as the leaf surface area per unit volume and $|U|$ is the wind velocity.

The governing equations were numerically solved using the semi-implicit method for a pressure-linked equation (SIMPLE) algorithm and a finite volume method in a staggered grid system [34]. The velocity components, U_i were defined at the center of the grid cell faces whereas the scalar variables were defined at the center of the grid cell. This approach is more numerically accurate and stable than the grid system that stores all variables at one grid point [37]. The combined advection-diffusion terms in the governing equations were discretized using a power-law differencing scheme, which was proven to provide accurate approximations [37]. A fully implicit scheme with first-order accuracy was applied for the time integration [34].

2.2 Model Validation

The experiment was conducted in an open-loop wind tunnel (WT) located at Malaysia–Japan International Institute of Technology (MJIIT), Universiti Teknologi Malaysia (UTM). The wind tunnel cross-sectional area at the measurement location is W x H x L = 1.35 m x 1.0 m x 9.0 m. The building model dimensions are W x H x L = 0.47 m x 0.044 m x 0.6 m. Scaled building models (1:250) were produced by PLA (Polylactic Acid) with a filament diameter of 1.75 mm. The product density was 30% according to the building layout by using a three-dimensional printer with a nozzle size of 0.08 mm. Exact building shapes with no complex geometry were generated without considering detailed features such as windows, balconies, openings, or roof shapes. Thus, the roughness of the building is not affecting the flow. The standard of landscape elements, including trees or other vegetation, was adopted during the test model preparation. The maximum blockage ratio is 2%, which is below the recommended maximum of 3%, which is necessary to prevent wind tunnel wall effects [38].

The inflow condition is described by a power-law profile with exponent 0.11, which represents open surface terrain measured over smooth water surfaces according to Sisterson and Frenzen [39]. The approach flow reference wind speed, U_{ref} was 8.46 m/s at building height, H = 11 m. The pitot tube calculated the wind velocity according to Dwyer Application Guide by measuring the differential pressure inside the wind tunnel; the equation used for this calculation is given as Eq. (13) below [40]

$$V = 1.4123\sqrt{\frac{P_D}{\rho_{air}}} \tag{13}$$

where 1.4123 is the constant value, P_D (Pa) represents the differential pressure from the pitot tube, and ρ_{air} (kg/m^3) is the air density inside the wind tunnel. The wind velocity at a certain location was measured using a hot wire anemometer. The hot wire was set to collect data at the measurement frequency of 1 kHz for 10 seconds. A calibration curve for hot wire was obtained using polynomial curve fitting, shown in Eq. (14) below

$$U = AE^4 + BE^2 + C \tag{14}$$

where *E* is the corrected output voltage constant while *A*, *B*, and *C* are calibration constants. Once the calibration was completed, the pitot tube was removed, and the hot wire was moved to the target position. The wind speed was set constant at 11 m/s (the minimum speed required for the fan to be stable) inside the wind tunnel.

The measurement of the streamwise velocity without the building and tree was performed at the center of the test section (y = 0) and started at the vertical position z = 7 mm from the wind tunnel floor. Then the measurement height was vertically increased at the intervals of 1 mm (in the height range of 7 mm ≤ z ≤ 230 mm) with 223 measured points. To correlate the wind profile against building height in the wind tunnel and CFD simulation, Figure 2 shows the wind profile of the wind tunnel without the building model at the streamwise positions. From the wind profile, the calculation of the wind shear coefficient can be determined from the power law as below [41]

$$\alpha = \frac{\ln(v_2)-\ln(v_1)}{\ln(z_2)-\ln(z_1)} \tag{15}$$

where v_1 represents the wind speed at the reference position $z_1$and v_2 represents the wind speed at the elevated position z_2.

As mentioned previously, a power-law profile was imposed as the incoming velocity to represent realistic field conditions which required a theoretical validation [42,43]. Therefore, an appropriate inlet boundary condition of the wind profile against building height in the wind tunnel was plotted to ensure the proper configuration with the numerical model. As shown in Figure 2, good results were achieved for all incoming velocities, which provides a reliable foundation for further simulations. However, Figure 2 exhibits observable deviations, which is necessary to evaluate the relative standard deviation (RSD), to assess the accuracy of the results as displayed in Eq. (16) [20]

$$RSD = \frac{\sqrt{(v_1-\bar{v})^2+(v_2-\bar{v})^2}}{\bar{v}} \times 100\% \tag{16}$$

where v_1 is the wind-tunnel velocity, v_2 is the velocity from CFD simulation and $\bar{v}$ is the average of both. The RSD was measured at 2.44% and falls within an acceptable range.

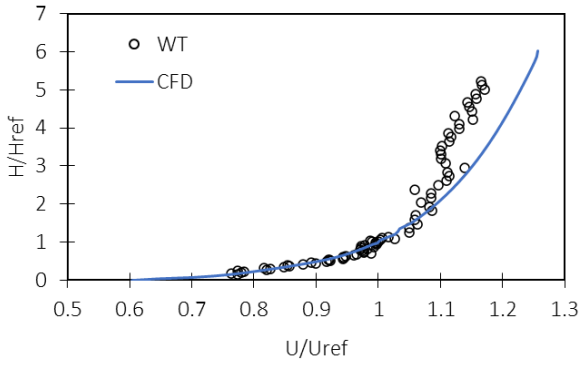

Fig. 2. Inflow wind from the measured wind tunnel (WT) and simulated (CFD) wind velocity, U normalized by U_{ref}

Measurements in the empty wind tunnel were made by comparing the results of inflow wind from CFD simulations and WT tests in Figure 2. The U/U_{ref} obtained by CFD shows a similar trend as WT as H/H_{ref} increased. Thus, it is indicated that the inflow wind in WT is similar and can be validated with the simulation result. For the setup arrangement of the model, the measurement started at 1H, 2H, 3H, and 4H, which H referred to as building height in the WT at 44 mm, by using Hot Wire Anemometer (HWA) as shown in Figure 3(a). The dimensions of each location measurement are shown in Figure 3(b). For each location of 1H, 2H, 3H, and 4H, the distance from the building is 44 mm, 88 mm, 132 mm, and 176 mm, respectively. The SG tree was added as a landscape in front of

the building according to the real condition in the site location, compute in the simulation, and modeled in WT. The tree diameter is 60 mm, and the height of both SG is 120 mm as shown in Figure 3(c).

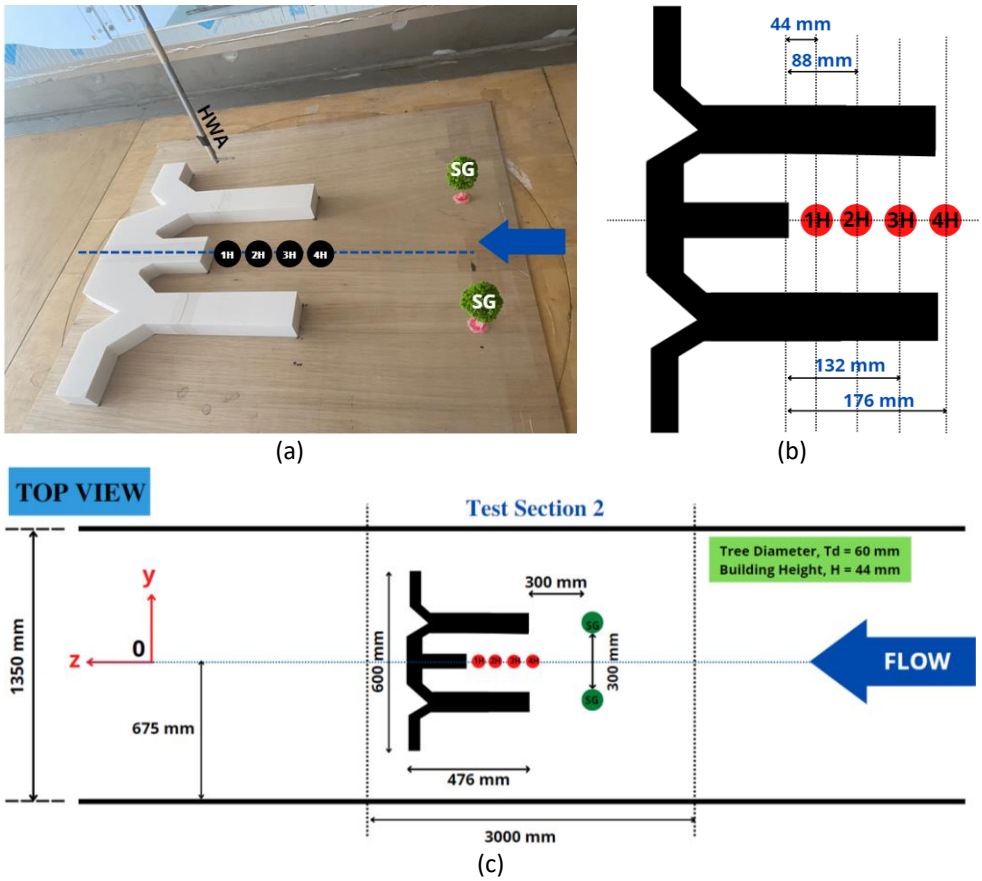

Fig. 3. Setup diagram of the (a) WT test section with building model and two SG tree models, and (b) details dimensions of distance 1H, 2H, 3H, and 4H, and (c) top view diagram of the model in the WT test section at streamwise measurement positions

Figure 4 shows the validation of normalized U/U_{ref} against H/H_{ref} between CFD and WT. The CFD results show similar behavior to those obtained from the WT experiment. This result indicates that the CFD model accurately captures the flow characteristics and patterns observed in the real-case condition represented by the WT. Therefore, the close agreement between the results from CFD and WT across the entire range of measurements suggests that the CFD simulations effectively replicate the physical phenomena and accurately predict the flow behavior of the system. The good results from the validation studies provide additional support and serve as a reliable tool for further analysis of CFD.

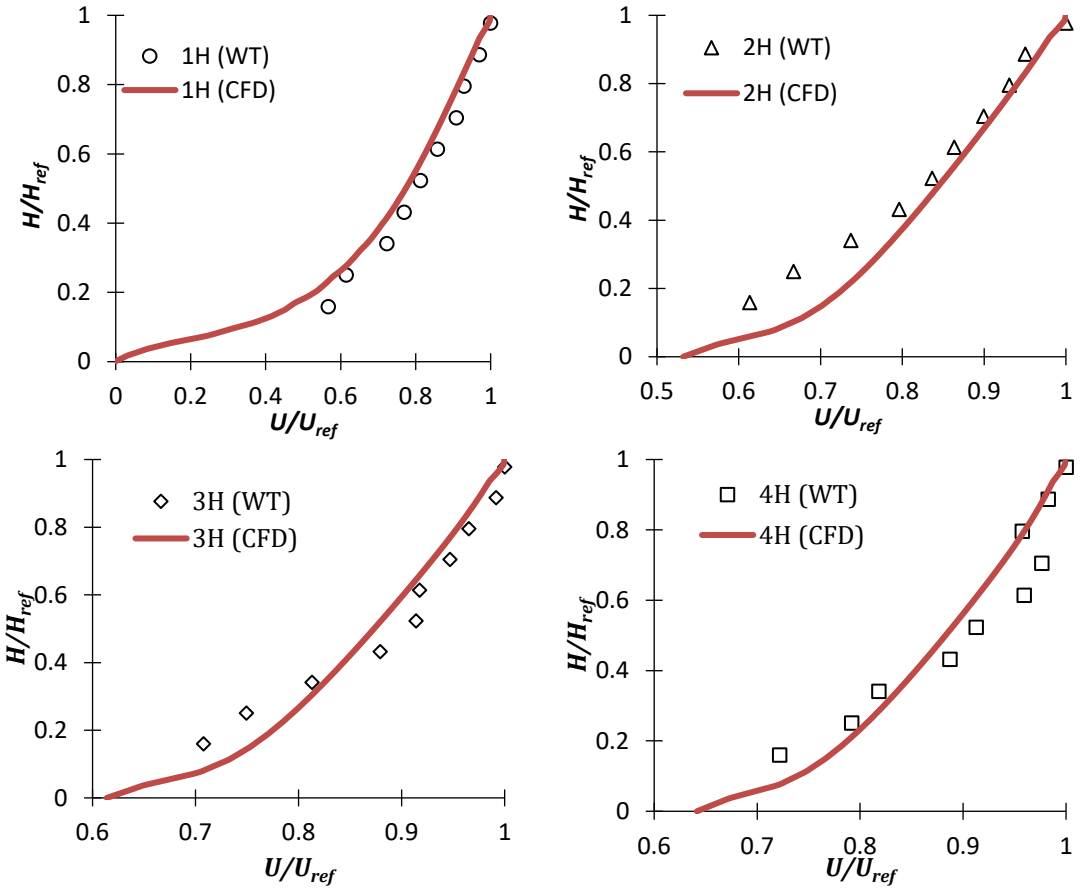

Fig. 4. Comparison of normalized U/U_{ref} against H/H_{ref} between CFD and WT at 1H, 2H, 3H, and 4H

2.3 Computational Domain and Grid

For the inlet plane, a power-law velocity profile was applied, as expressed by Eq. (17). The inflow profiles of the wind velocity (k and ε) were provided by the Architectural Institute of Japan (AIJ) as follows [25]

$$U(z) = U_{ref}\left(\frac{z}{H_{ref}}\right)^{\alpha} \tag{17}$$

$$k(z) = a(I_u(z)U(z))^2 \tag{18}$$

$$\varepsilon(z) = C_{\mu}^{\frac{1}{2}}k(z)\frac{U_{ref}}{H_{ref}}\alpha\left(\frac{z}{H_{ref}}\right)^{(\alpha-1)} \tag{19}$$

where U_{ref} = 8.46 m/s is the mean velocity at the reference height, H = 11 m, and α = 0.11. The power-law exponent was set to 0.11. The turbulence kinetic energy $k(z)$ in Eq. (18) and the turbulence dissipation rate $\varepsilon(z)$ in Eq. (19) were calculated from the velocity profile $U(z)$ with the model constant C_{μ} = 0.09 and a = 1 [25]. The geometric idealization of the Holiday Villa Beach Resort building is shown in Figure 5. The computational domain was based on the standard geometry stated in the AIJ guidelines for performing a CFD simulation of wind around buildings as shown in Figure 5(a) [25]. The height and width of the computational domain are 55 m and 285 m, respectively. The domain height was equivalent to 5H, where H = 11 m was the building height. The entire length of the domain was

418 m. The recommendation from AIJ intends to assure more realistic simulations of behind-building wake flows and prevent artificial acceleration of around-building flows near the boundary.

For the outside of the target area located in the numerical domain's center, we used a non-uniform grid system located from the center of the numerical domain (Figure 5(b)). Uniform grid cell sizes (cell numbers) were applied within the target area in the x, y, and z directions of 175 m, 198 m, and 11 m, which are 1.67 m (105), 1.58 m (125), and 0.28 m (40), respectively. The grid cells expanded in the x, y, and z directions at an expansion ratio of 1.8 from each boundary of the target area until the maximum grid cell sizes reached 3.89 m and 1.55 m in the x and y directions and 1.65 m in the z-direction. The grid cell numbers were 180, 180, and 100 in the x, y, and z directions, respectively, yielding respective domain sizes of 285 m, 418 m, and 55 m. The lateral and top boundaries were sufficiently far from the boundaries of the target area (horizontal, 5H, and 15H; vertical, 5H). The size of the first near-wall cell was chosen equal to 0.0025 m to keep the dimensionless wall unit (y^+) value in the log-law range, between 30 and 300. The computational grids contained 12.1 million cells and 6.8 million points in the domain, respectively.

The data of the prevailing wind from Northeast to East were used in the simulation as an input of the wind direction in CFD simulation, which was obtained at a height of 10 m from the Langkawi Weather Station, which was forecasted by the Malaysian Meteorological Department at Langkawi International Airport. The data was collected from 2015 to 2020.

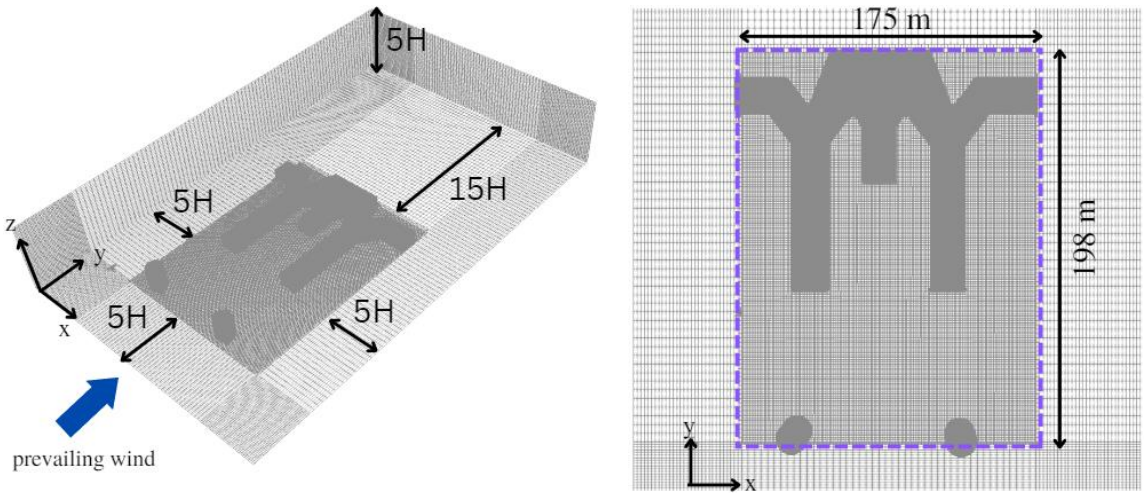

(a) (b)

Fig. 5. Figure of (a) computational domain with relevant distances and (b) top view of the computational grid on the building

Buildings were designed using SketchUp by referring to Google Earth and Holiday Villa Beach Resort's official website. To achieve realistic simulations, the parameters related to trees such as the tree's height, tree's diameter, tree's species, tree's optical porosity (Ø), and leaf area index (LAI) were measured during field measurement at the target area. The Ø and LAI of trees were determined using a fisheye lens as in Figure 6 and VitiCanopy software. However, for drag coefficient (Cd) we obtained values from the literature due to the instrument limitation for this parameter. There are two types of tree species planted along the building area, which are Syzygium Grande (SG), and Casuarina equisetifolia (CE). The SG tree was planted along the coastline area and in front of the building resort, which considers a landscape for the resort and was included in the simulation model (Figure 5(b)). Meanwhile, CE was planted behind the building resort along the roadside, which is not included in the simulation.

However, the CE tree will be planted in a single row and double rows, as a new tree model in CFD simulation to replace the SG tree's landscape. A new tree model will be acting as windbreak fences around buildings to improve pedestrian wind comfort for local people and tourists at the resort. In this study, the Ø of SG and CE were 20.5% and 49.9%. Meanwhile, the LAI of the SG (Figure 6(a)) and CE (Figure 6(b)) trees were 2.185 and 0.927; the Cd of the SG and CE was set at 12.48 and 1.56, according to Jian *et al.,* [44] which depends on the tree's porosity. All simulations were run for a total physical duration of 100 s with a time step of 0.1 s. Zero-gradient conditions were applied at the lateral and outflow boundaries, and wall functions suggested by Versteeg and Malalasekera [45] were applied at the solid wall boundaries. The CFD model was integrated up to 3600 s in 0.5 s increments.

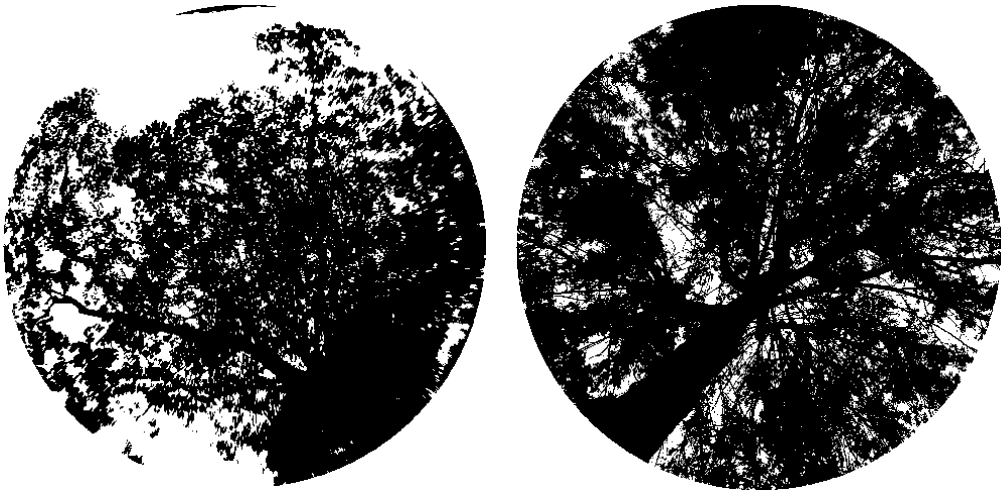

(a) SG (b) CE

Fig. 6. The Ø and LAI of (a) SG are 20.5% and 2.185, and (b) CE are 49.9% and 0.927

2.4 Simulation Setup and Other Computational Parameters

An outline of the simulation setup applied is provided in Table 1. The wind simulations were performed by solving the incompressible, three-dimensional steady RANS equations with the finite volume method. Turbulent closure was provided by the RNG k-ε turbulence model and the SIMPLE algorithm handled the pressure-velocity coupling ensuring that the continuity equation is satisfied. Second-order discretization schemes were used for the spatial discretization, including the convective terms. The iterative convergence criteria were that the scaled residuals should drop four orders of magnitude for k, ε, and each cartesian component of U. The convergence criterion for P was relaxed to 1.0×10^{-4}. This was done to speed up the simulations, as reaching a residual drop of four orders of the magnitude required significantly longer simulation time. The relaxation of the convergence criterion did not impact the wind velocity magnitude at the pedestrian level in the built area investigated in this paper.

These criteria were met for all simulations presented. The simulations were conducted using the OpenFOAM (version 5.x) toolbox, which is an open-source CFD software package. An overview of the boundary conditions used is presented in Table 2. Wind velocity data obtained during the wind tunnel experiment by Miyazaki and Tominaga [46] served as input values for the *y*-component inlet velocities (u_y) whereas the other velocity components (u_x and u_z) were assumed to be zero. The pressure was also given a zero gradient for the inlet, top, ground, and lateral sides, as well as an urban block with a uniform outlet value as the pressure was assumed to be constant. For the other regions in the domain, the outlet flow was given a fully developed flow condition, namely

pressureInletOutletVelocity. The slip conditions were set for the top and lateral side regions, the no-slip condition for the ground and the urban block, and the near-wall conditions for ε and k (i.e., *epsilonWallFunction* and *kqrWallFunction* respectively). The initial values inside the domain for all parameters were set to zero.

Table 1
Overview of simulation setup

Feature	Type
Software	OpenFOAM version 5.x
Equation system	3D incompressible steady RANS
Solver	Generalized geometric Algebraic Multi Grid, GAMG solver (*P*) smoothSolver ($U, k, \omega, \varepsilon$)
Turbulence model	RNG k-ε
Pressure-velocity coupling	SIMPLE algorithm
Convergence criteria	Residual drop to 1.0×10^{-4}
Discretization schemes	Second-order
Boundary conditions	see Table 2

Table 2
Overview of boundary conditions applied

Patch	Type
Sides	Slip wall
Inlet	Power-law velocity profile
Outlet	Constant pressure
Ground	No slip wall
Buildings	No slip wall
Top	Slip wall

2.5 Production of Pedestrian Wind Comfort Grade

Since there are many standards for determining wind comfort, the guideline from NEN 8100 was adopted in this simulation. The provided criteria of NEN 8100 encompass various activities related to occupancy to evaluate the potential threshold values of wind velocity that establish the comfort standards for beachfront open-building resorts. In this standard, the wind velocity discomfort threshold, U_{THR} is set at 5 m/s for all levels of pedestrian activities, and the local wind comfort is assessed based on the possibility of the wind velocity exceeding this value [47]. Table 3 tabulates the criteria for wind comfort according to the NEN 8100 standard. $P(U_{THR})$ is the probability value for wind velocity to exceed the threshold wind velocity, U_{THR} of 5 m/s. To determine the exceedance probability in this study, three steps are required according to Blocken *et al.,* [48]

i. Obtain the wind speed ratios ($\gamma = U/U_{ref}$, 11 m) as a design-related contribution from CFD simulations. The reference wind speed value (U_{ref}, 11 m) is the value of the inlet wind speed profile at a height of 11 m;
ii. Convert the threshold wind speed at the pedestrian level to a threshold wind speed at a height of 11 m (U_{THR}, 11 m = U_{THR}/γ);
iii. Determine the percentage of time that the threshold value for the mean wind speed at 11 m is exceeded according to the wind statistics of the location of interest. This 11 m height from the ground is determined based on the long-term experiments performed to prepare Dutch Practice Guideline NPR 6097 [49].

Table 3
Pedestrian wind comfort criteria used in the study, based on NEN 8100 [50]

P (U_{THR} > 5m/s) %	Grade	Activity			Comfort criteria
		Traversing	Strolling	Sitting	
< 2.5	A	Good	Good	Good	Sitting long
2.05 - 5.0	B	Good	Good	Moderate	Sitting short
5.0 - 10	C	Good	Moderate	Poor	Walking leisurely
10 - 20	D	Moderate	Poor	Poor	Walking fast
> 20	E	Poor	Poor	Poor	Uncomfortable

3. Results and Discussion

3.1 Existing Conditions at the Pool Section

Figure 7 shows the wind flow at pedestrian height level from the top view of the building. As observed, the pool section (in yellow dash box as in Figure 7) experienced a velocity of more than 5 m/s, which lies in moderate breeze according to the Beaufort wind scale [35]. The assessment of wind conditions around the building and the comfort of pedestrians was specifically focused on the pool area, which serves as a public recreational zone. The wind velocity in Figure 7 at the windward side of the building changed drastically in the pool section.

These sections had negative wind velocity until the wind was near the windward side of the building, where a local peak occurred due to the small vortex region generated in front of the building and near the ground. This vortex was caused by a downward deflection of the flow across the front of the building to the ground, where it deflected again, resulting in a near-bed flow in the opposite direction of the incoming wind direction. Investigations by Pourteimouri *et al.,* [36] showed that the wind speed increases steadily with increasing distance from the reattachment point until it eventually reaches the undisturbed wind velocity magnitude. Additionally, the findings show that the long building requires a longer distance for the wind to reach the undisturbed wind velocity magnitude.

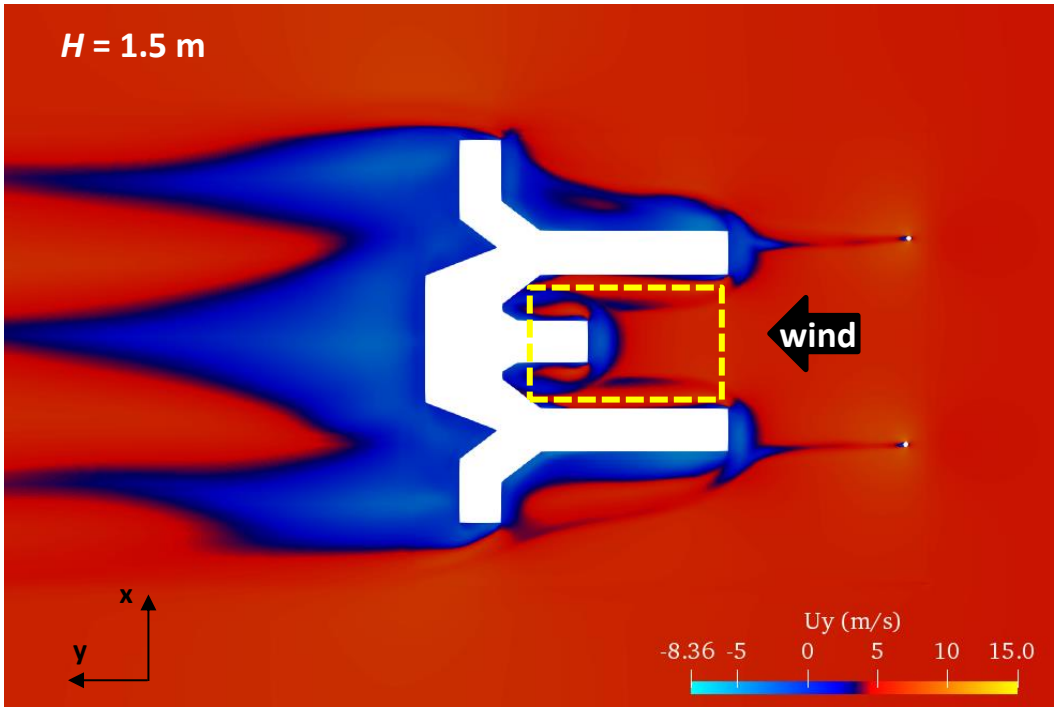

Fig. 7. The wind flow at pedestrian height from the top view of the building

Since there are many standards for determining wind comfort, the guideline from NEN 8100 was adopted in this simulation [50]. The provided criteria of NEN 8100 encompass various activities related to occupancy to evaluate the potential threshold values of wind velocity that establish the comfort standards for beachfront open-building resorts. In this standard, the wind velocity discomfort threshold, U_{THR} is set at 5 m/s for all levels of pedestrian activities, and the local wind comfort is assessed based on the possibility of the wind velocity exceeding this value [47]. Referring to Table 3, it tabulates the criteria for wind comfort according to the NEN 8100. The probability of U_{THR} is the probability value for wind velocity that exceeds the threshold wind velocity, U_{THR} of 5 m/s. The standard was defined as five quality grades of wind comfort. The comfort criteria were divided into several activities, where each was associated with a quality grade. This helped to assess the comfort of the resort guests, especially at the pedestrian level to perform these activities.

Figure 8 represents the current condition after calculating the percentage exceedances probabilities for wind nuisance at the prevailing wind of the building and quality classes for wind comfort assessment according to NEN 8100. The map with wind classes at pedestrian level in current condition (Figure 8(b)) showed rather large areas with quality Class C in yellow color, which indicates up to 27% (red color) of P(U_{THR} > 5 m/s) around the building as in Figure 8(a). These areas have a good wind climate for traversing and moderate wind climate for strolling and poor for sitting. Since the building resort is a place for leisure and tourists spot, it is typically a place for strolling and sitting; thus, steps should be taken to improve the wind condition in these areas, so that it is at least good for strolling and sitting as in Class A or B. Moreover, the small red color in Figure 8(b) indicates the SG tree which resembles a landscape in front of the building.

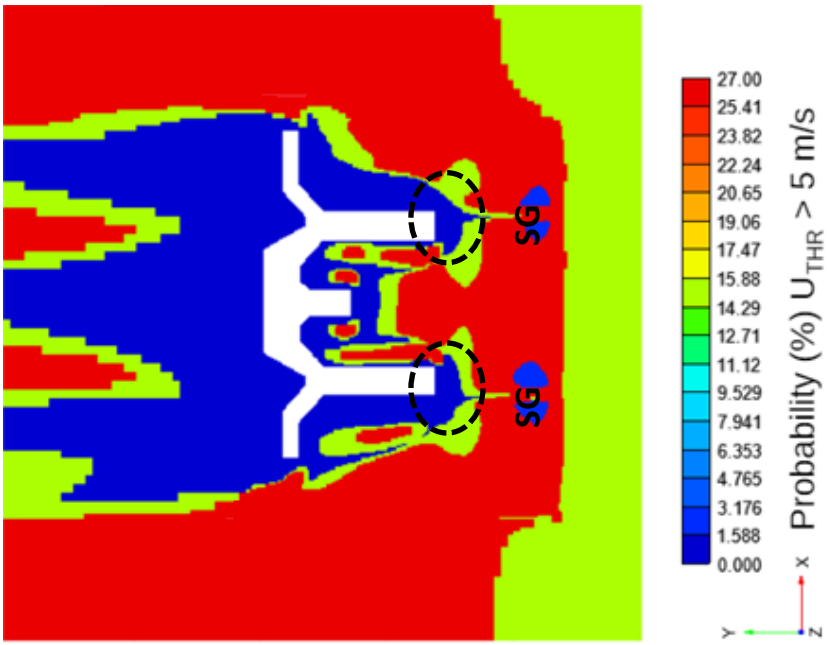

(a)

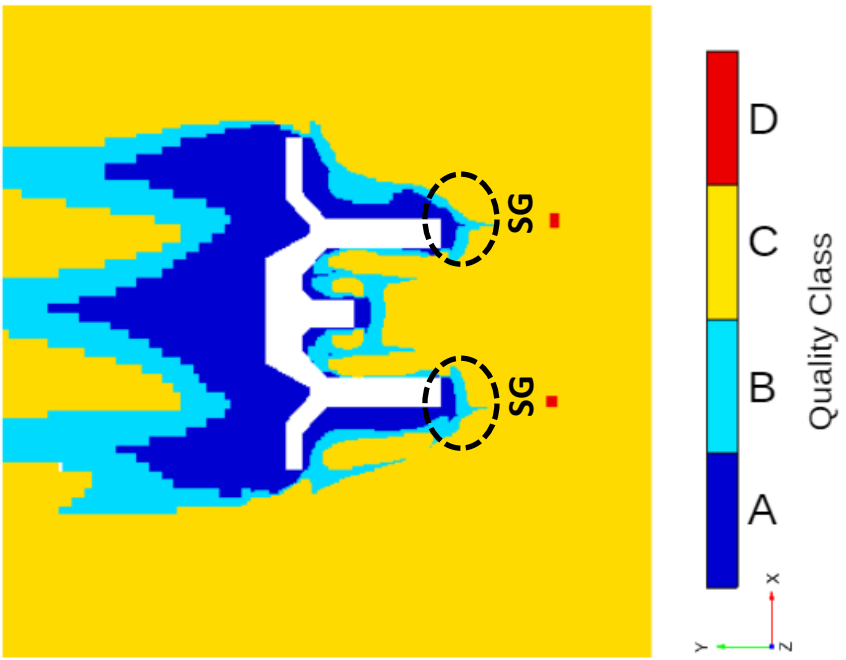

(b)

Fig. 8. The (a) exceedance probabilities for wind nuisance and the accompanying (b) quality class according to the Dutch Standard NEN 8100 were measured at 1.5 m height

The streamwise velocity and turbulent kinetic energy were measured at the distance of 1H, 2H, 3H, and 4H upstream of the building as in Figure 9. The simulation results in the pool section, which is an open space, show that U/U_{ref} increased as the distance from the building increased. For example, at the distance of 1H, U/U_{ref} had the lowest value which was approximately zero until the wind was close to the building's windward face Figure 9(a), where a local peak occurs due to the small vortex region that forms in front of the building and close to the surface. Moreover, a decrease in k/U_{ref}^2 was observed, where k/U_{ref}^2 was nearly zero, as a consequence of wind velocity reduction causing potential turbulence energy reduction in the downwind canopy [51].

Conversely, introducing a vegetative windbreak in front of a building, changed the structures of the flow field and significantly impacted the velocity, as the trees created patches at different turbulent intensities [52]. To enhance natural ventilation and improve pedestrian wind comfort, particularly in leisure and recreational areas at the building resort, it was crucial to undertake measures that addressed these effects. One of the effective methods involves the implementation of natural windbreaks that were strategically arranged around the building to provide better wind comfort. Further investigation and action were conducted to optimize these measures and promote a more favourable environment.

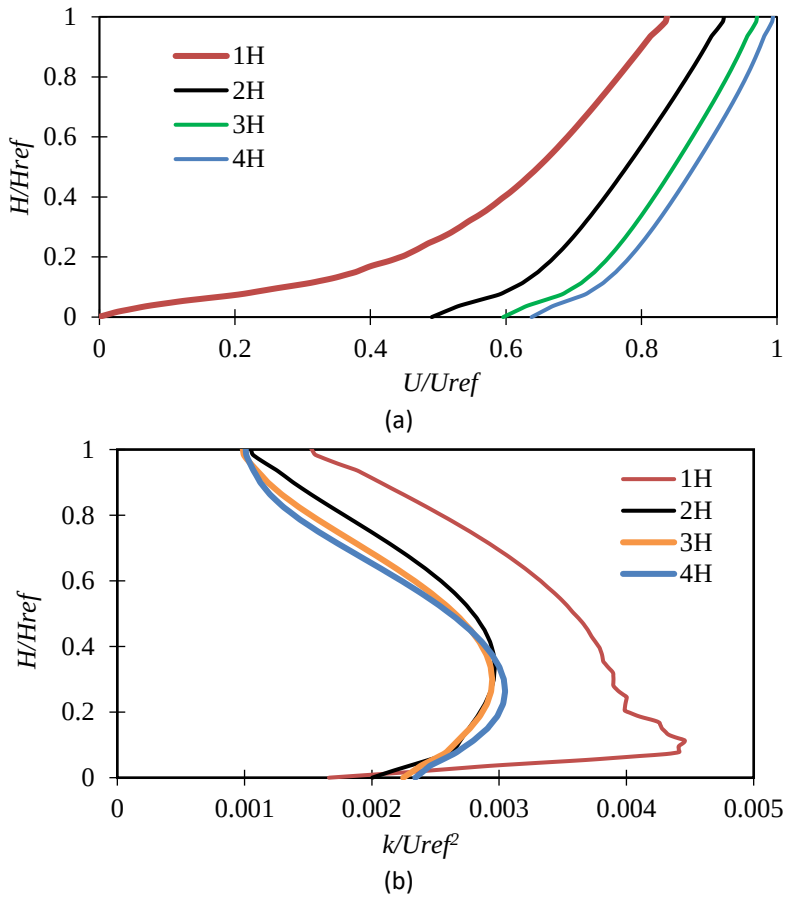

Fig. 9. The vertical (a) normalized U/U_{ref}, and (b) normalized k/U_{ref}^2 at four distances in the pool section

3.2 Single Row Windbreak Simulation

The CE trees have the potential to act as windbreak trees that could minimize the strong wind effects resulting from the tropical storms that hit Langkawi Island every year. In practice, windbreaks are often built into double or triple-row arrangements to reduce turbulence intensity and increase the shelter effect [53]. In this section, a numerical investigation analysis of the windbreak effect by a single row of CE trees was discussed. Figure 10(a) illustrates the top view of the building resort and the potential windbreak location of CE trees which are located 30 m from the beachline and 74 m from the building and swimming pool, which was a similar distance inside the domain in CFD. The distance between the canopy of the CE trees was 4 m, as shown in Figure 10(b). This distance was chosen based on the guideline for the CE tree positioning within crop rows [54].

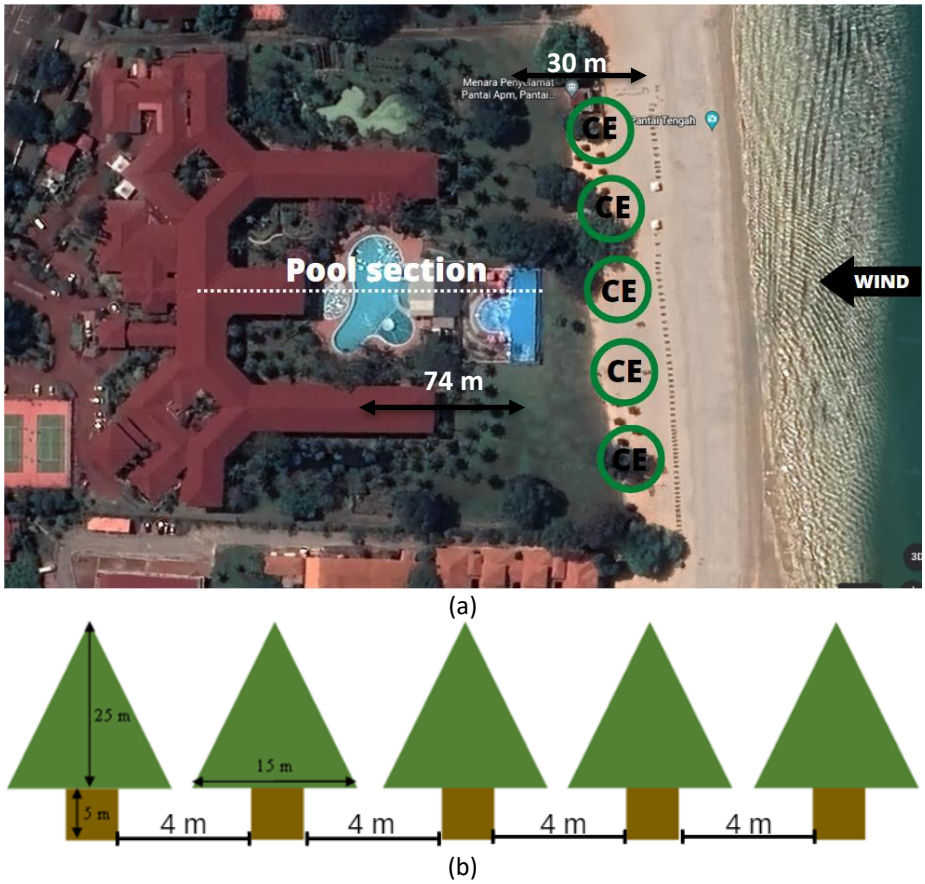

Fig. 10. The view of the (a) building resort and potential windbreak location, (b) canopy distance of the CE tree models in the simulation

To predict the wind velocity behind a windbreak, it was crucial to understand the wind flow around the windbreak, the mechanism, that drives it, and the interaction between flow and windbreak. According to Dong *et al.,* [55], the effectiveness of windbreak was related to the flow characteristics in several regions and divided into main regions which were; (i) a separated region directly behind the windbreak, (ii) a recovery region where the influence of the windbreak was negligible, and (ii) a mixing region between the separated and recovery regions. However, Judd *et al.,* [53] introduced a simplified version of the different regions behind windbreak in a modified form. Figure 11 shows the flow division of a two-dimensional flow field around the windbreak. The flow field was evaluated based on building height, H, and windbreak height, Ht. At the upwind flow of the windbreak, region A was called the approach flow, which was characterized by upwind terrain conditions. Downwind of Region A, the flow was divided into several regions, which were Region B was known as displaced flow, and Region C as bleed flow. Following the flow downstream, there will be a quiet zone in the lee of bleed flow which was in Region D.

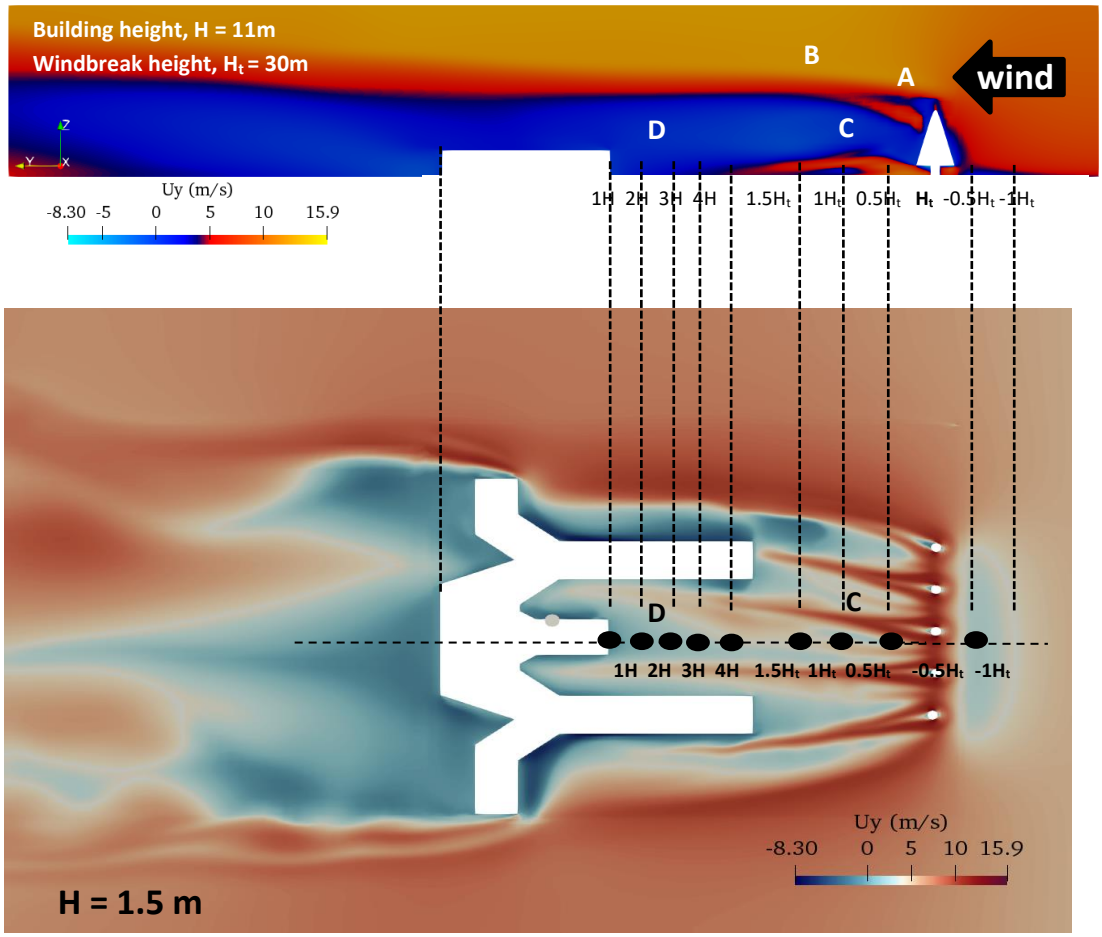

Fig. 11. The view of the (a) building resort and potential windbreak location, (b) canopy distance of the CE tree models in the simulation

The velocity curves in the pool section, for the case of a windbreak composed of a single-row windbreak, was shown in Figure 12. As can be noticed, the graph was configured simultaneously with the no-windbreak situation labeled as "*no tree*." In the case of no tree, the inlet velocity showed a power-law boundary layer profile. A single row reduces the velocity increased as the distance from the building increases. To assess the accuracy of the results, the average relative standard deviation was calculated to calculate the average reduction of U/U_{ref} at the pedestrian height for various locations. The average reduction of U/U_{ref} at each location, were as follows; 1H = 53.18%, 2H = 55.94%, 3H = 57.78%, and 4H = 59.89%. The average reduction of U/U_{ref} in this study aligned with findings from Jian *et al.,* [44] that mentioned wind profile curves were increased as the distances and height away from the tree's canopy.

About more than 50% reduction of U/U_{ref} for single row windbreak occurred due to a large scale of wind approached from displacement flow (Region B) which causes a marginal increase of velocity lateral to the tree. Meanwhile, a larger part of wind flow penetrates the canopy and rapidly decreases its velocity as it passes through the porous media known as bleeding flow as in Region C. These results were consistent with Khodayari *et al.,* [56], in which the wind reduction was increased as it reaches $1.0H/H_{ref}$ due to the maximum expansion of the windbreak canopy level. As shown in Figure 12(a), the U/U_{ref} at 1H decreased rapidly to approximately zero due to the vortex formed at the windward side of the building, and as a result, U/U_{ref} changed drastically.

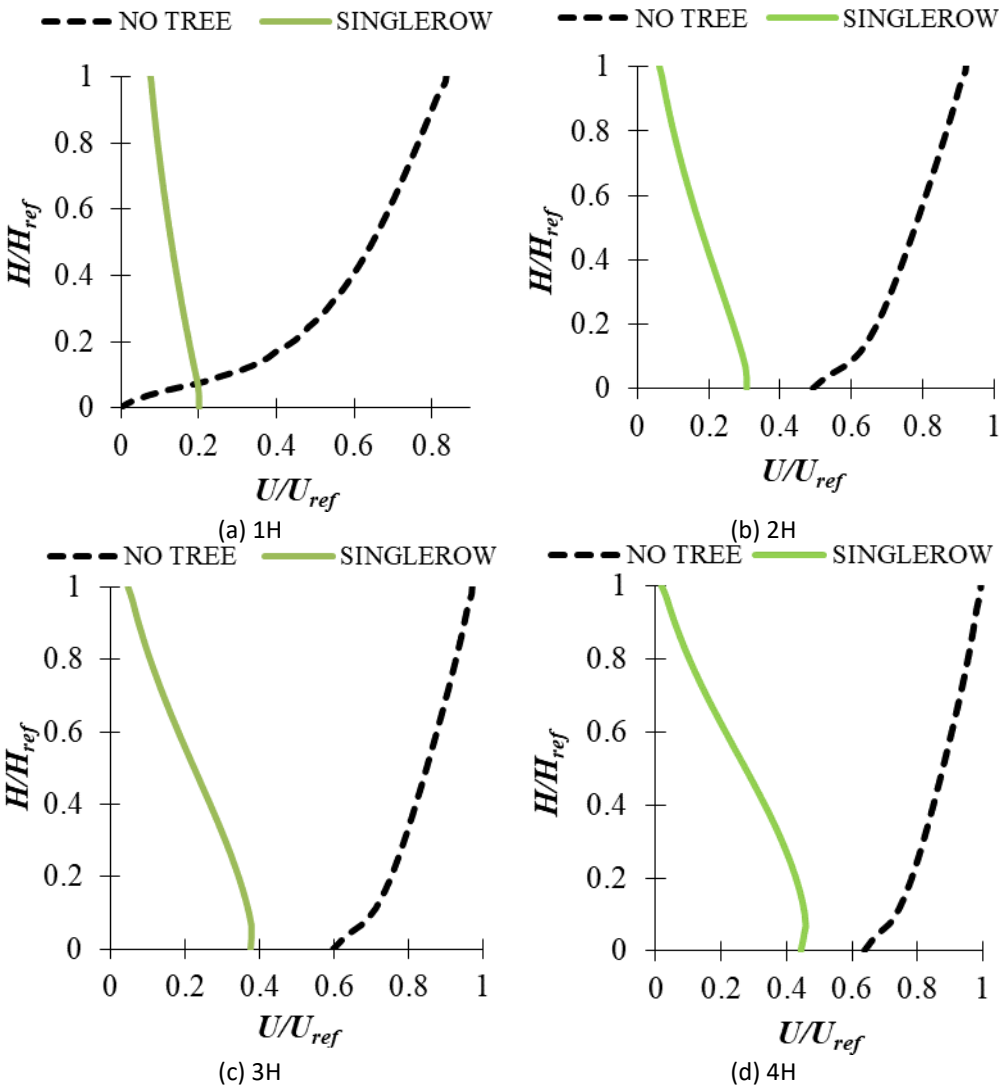

Fig. 12. The view of the (a) building resort and potential windbreak location, (b) canopy

Figure 13 shows the vertical U/U_{ref} and k/U_{ref}^2 against H/H_{ref} at the pool section with various distances. The k/U_{ref}^2 for a single row indicated higher turbulence compared with the no tree as its distance increased from the building wall. The increment of k/U_{ref}^2 for 1H, 2H, 3H, and 4H were based on average relative standard deviations which were 57.58%, 60.09%, 59.84%, and 58.98%. The presence of the tree changed the structure as the trees created patches of different k/U_{ref}^2 intensities. The k/U_{ref}^2 was observed to increase at the tree's top and bottom, and the flow field was mostly modified by the velocity field [57].

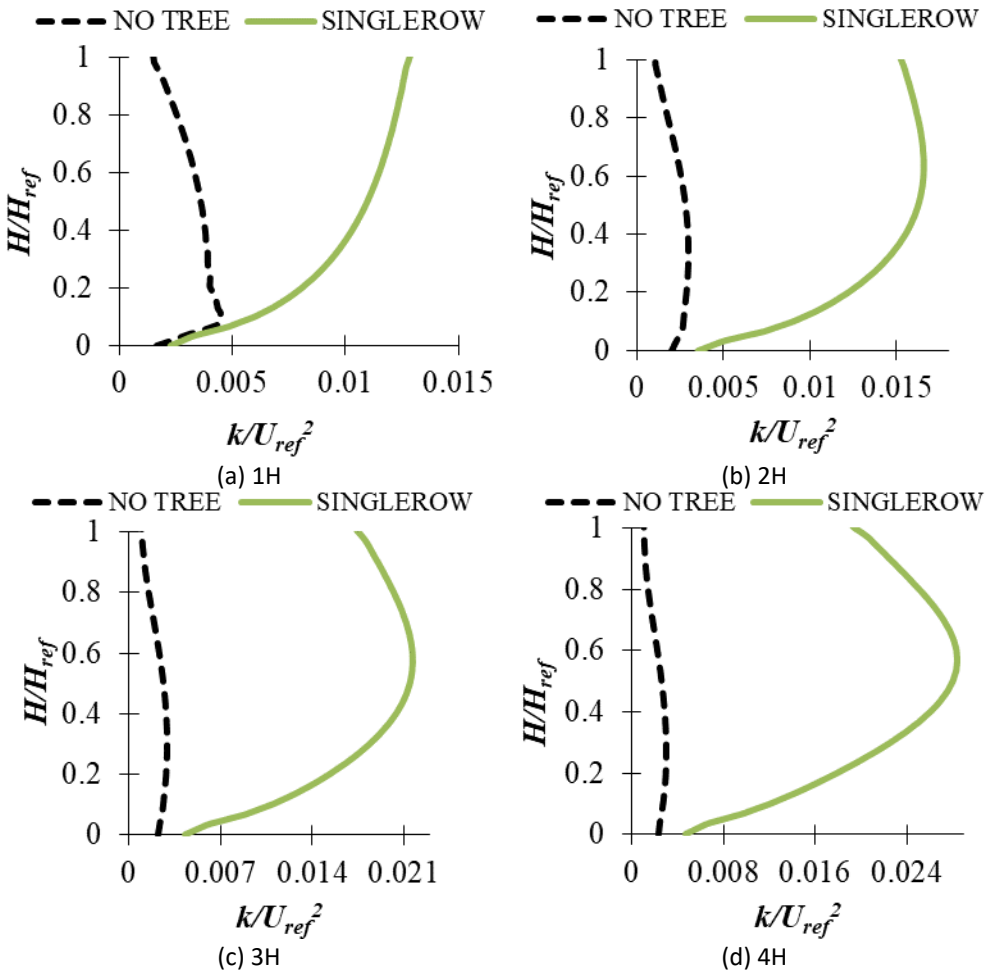

Fig. 13. The vertical U/U_{ref} and k/U_{ref}^2 against H/H_{ref} at the pool section with various distances of (a) 1H, (b) 2H, (c) 3H, and (d) 4H

The airflow around a single row behind a tree at the leeward side was illustrated in Figure 14. In the graph, H_t was referred to as a tree height that was 30 m. The dashed line referred to a trunk and canopy height that were 5 m, and 15 m. As observed, closest to the tree, the U/U_{ref} at $0.5H_t$ had the highest wind (≈ 1.26) compared to $1.0H_t$ (≈ 0.46) and $1.5H_t$ (≈ 0.43) at the trunk height level. This was due to the high stream from the prevailing wind penetrating through the porous barrier within a short distance downward of the tree, which created the standing vortex behind the tree, which began to merge with the flow crossing over from the top and sides of the tree and reduced the wind at 0.15 H/H_t with 0.8 U/U_{ref} which known as bleeding flow in Region C.

Moreover, the presence of a single-row windbreak altered the magnitude of wind flow wave motion, which propagated upward from the top of the canopy, or a wake generated by the collision between the wind flow and the trees. This motion impact from the reduction of wind exerted by the drag force from the canopy on the wind flow, while the propagation was due to mass conservation. As a result, the flow circulation was disturbed by the trees, which broke the wave motion into smaller eddies, where the impact of trees results in a reduction of k/U_{ref}^2 at 0.5 H/H_t as in Figure 14(b).

Specifically, the wind velocity at leeward of a windbreak at locations of $0.5H_t$, $1.0H_t$, and $1.5Ht$ was lowered compared to the windward side of a windbreak at locations of $-0.5H_t$ and $-1.0H_t$ as shown in Figure 14(a). This was due to the blocking nature of the vegetation which channelled the wind towards the building, leading to higher wind reduction in those areas [58]. The findings were aligned with Su *et al.,* [59] demonstrated that the higher reduction of wind velocity on the leeward side of windbreak was associated with the influence of turbulent kinetic energy, especially around

the trunk, which the blocking effect from the trunk lowered the value of turbulent, thereby weakening its intensity.

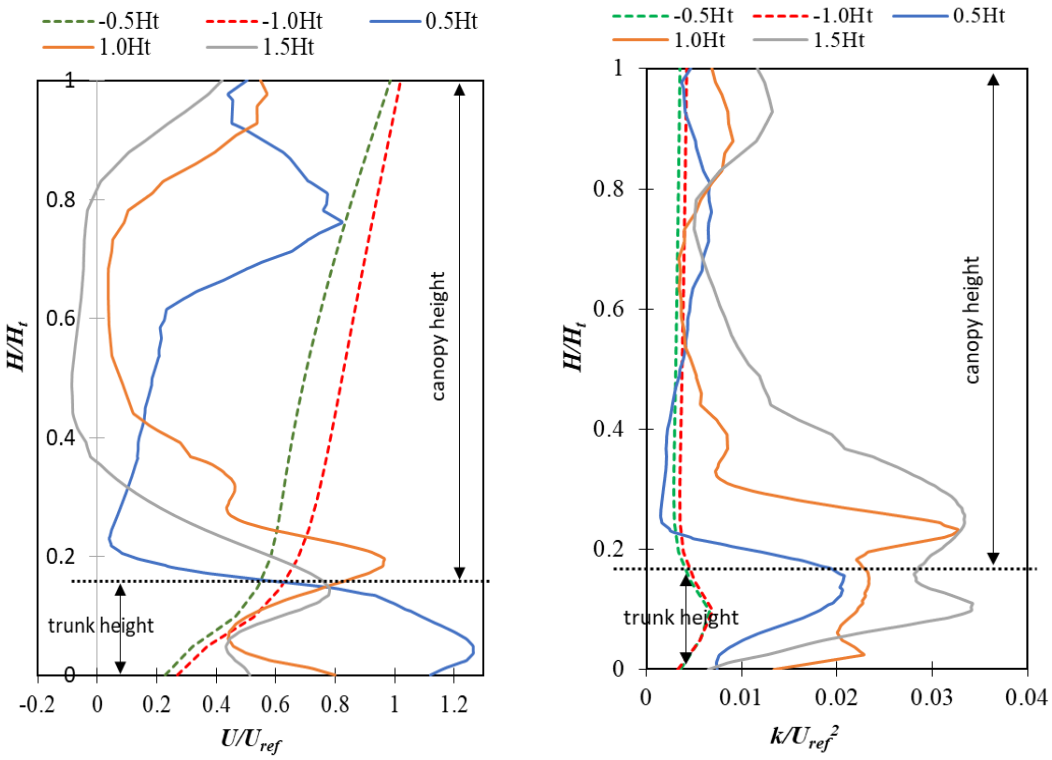

Fig. 14. The vertical (a) U/U_{ref} against H/H_t, and (b) k/U_{ref}^2 against H/H_t, in the pool section

To evaluate the quality of wind comfort in the presence of a single-row tree, the assessment of NEN 8100 was shown in Figure 15. Figure 15(a) shows the quality class according to the Dutch Standard NEN 8100. The colors in the figure represented different comfort classes. The dark blue color corresponded to Class A, the light blue color corresponded to Class B, the yellow color corresponded to Class C, and the red color corresponded to Class D. Classes C and D were classified as poor for walking and sitting, indicating that these classes should be avoided when considering the results. The results indicated that within the pool section, two quality classes were observed which are Class B and Class C. Additionally, Class A was identified near the building wall along the pool section.

To further identify the value of the probability of comfort class in, Figure 15(b) shows the JPDF of exceedance probability that was more than threshold wind, P(U_{THR}) which is 5 m/s. Figure 15(b) illustrated different colors that represented different levels of P(U_{THR}). The blue color indicated the lowest P(U_{THR}), which was less than 3%. On the other hand, the red color represented the highest P(U_{THR}) value, exceeding 10%. Results showed that P(U_{THR}) of Class C was observed at about 10% in the pool section, while Class B has a value of 0.5%. The percentage of the classes for each quality was 46% for Class A, 12% for Class B, 39% for Class C, and 3% for Class D. Therefore, the presence of the single-row tree indicated good conditions for traversing and strolling at the pool section around the resort's building. However, it should be acknowledged that the suitability of the other activities may vary, and further assessment was crucial to evaluate the optimal level of comfort.

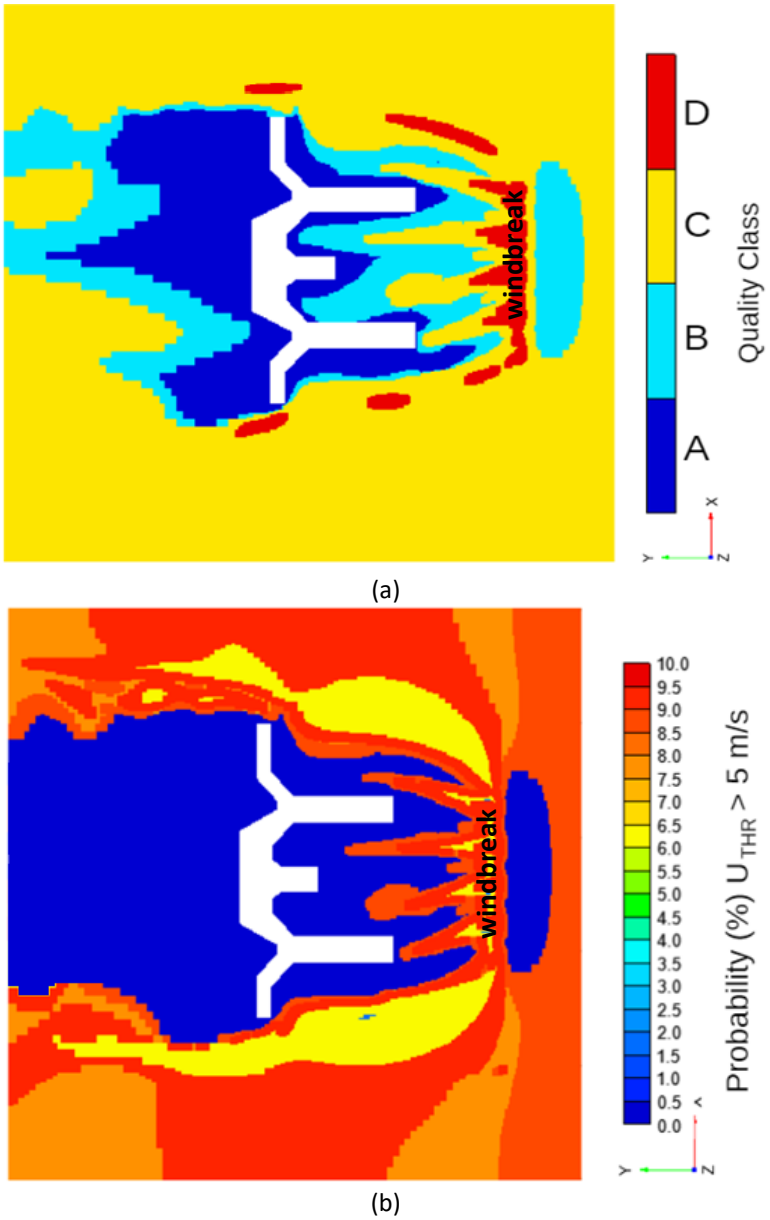

Fig. 15. The joint probability distribution function of (a) quality class according to the Dutch Standard NEN 8100 and (b) exceedance probabilities for wind nuisance for a single row windbreak tree measured at 1.5 m height

3.3 Staggered Double Row Windbreak Simulation

In the simulation, the staggered distribution of double rows arrangement was applied. Figure 16 shows the canopy distance of the staggered double rows of CE tree models, in which the distance between the trees in each row was 4 m and the second rows of each tree were planted at 45˚ angle from the beach line. The distance was chosen based on the guideline for the CE tree positioning within crop rows and the most common arrangement of windbreak in practical applications [54,60].

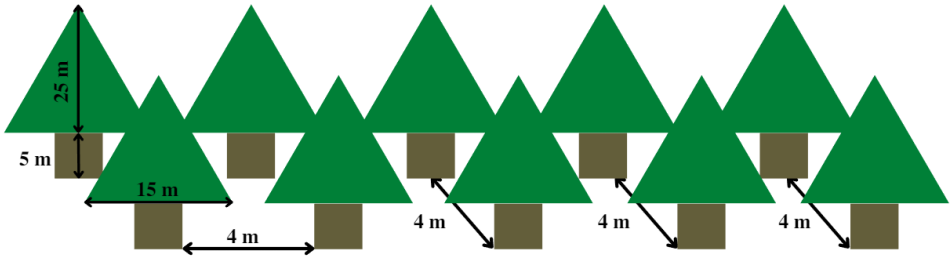

Fig. 16. The canopy distance of the staggered double rows of CE tree models in the simulation

Figure 17 displayed the top view of windbreak locations consisting of staggered double rows installed in front of the building resort. From the observation, the CE trees were positioned at 10 m from the beachline and 74 m from the building wall and swimming pool, which was consistent with the distance implemented within the entire domain. Meanwhile, Figure 18 demonstrated the velocity distribution of the two-dimensional flow field around the windbreak simulation at 1.5 m height. As observed, the gap between the trees within a row created a channel effect, that caused the wind trapped between these spaces. This resulted in wind velocity reaching up to 16.6 m/s in between the tree trunk.

Fig. 17. The view of the building resort and double rows windbreak location

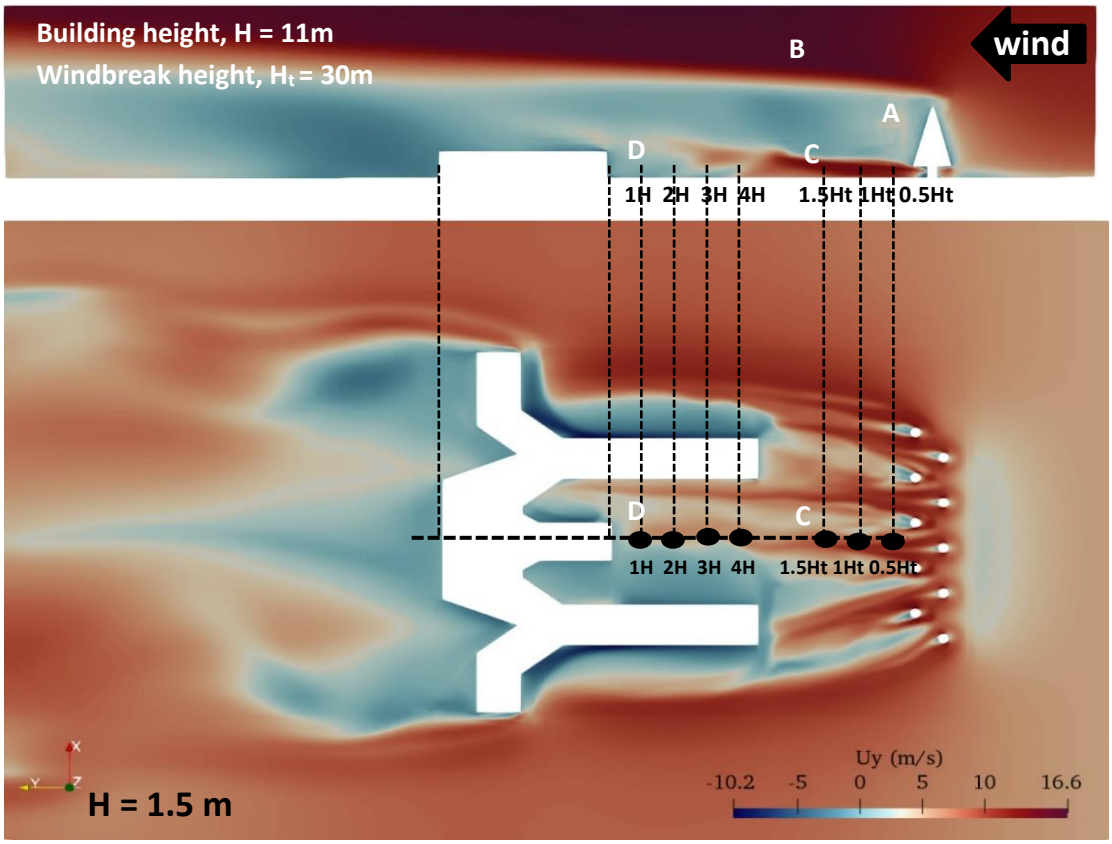

Fig. 18. The velocity distribution of the two-dimensional flow field around the windbreak simulation at 1.5 m height

The species of trees installed in a windbreak had a significant impact on its overall performance. Windbreaks comprised of numerous tree and shrub species planted in rows vary greatly in their capacity to protect against windstorms. The density or porosity of the windbreak, instead of the number of rows, determines the amount of protection around the building. Single-row windbreaks were known as the most efficient in reducing wind velocity than the second and third rows located in its leeward [60]. Fortunately, a canopy with several rows generally showed better results in lowering wind velocity than a canopy with only a single row and providing a well-protected area inside the rows, which was significant in actual windbreaks engineering applications.

Therefore, to identify the characteristics of wind flow behind the windbreak in staggered double rows, Figure 19 shows the vertical U/U_{ref} against H/H_{ref} at the pool section with different distances in the simulation. It is noted that in the graph, the staggered double rows configuration was labeled as "DROW(STG)", while the absence of any windbreak was labeled as "NO TREE". The wind reduction based on the averaged relative standard deviation of staggered double rows and without windbreak at the pool section at 1H, 2H, 3H, and 4H were determined to be 48.14%, 49.06%, 47.82%, and 46.56%, respectively. Figure 19(d) shows the lowest wind reduction at 4H from $0.6H/H_{ref}$ to $0.8H/H_{ref}$ was due to the presence of the trees, where oscillations in airflow occurred. These oscillations were caused by increased fluid entropy in the wake and within the trunk [61]. Thus, this led to an increased value of U/U_{ref}, as H/H_{ref} increased.

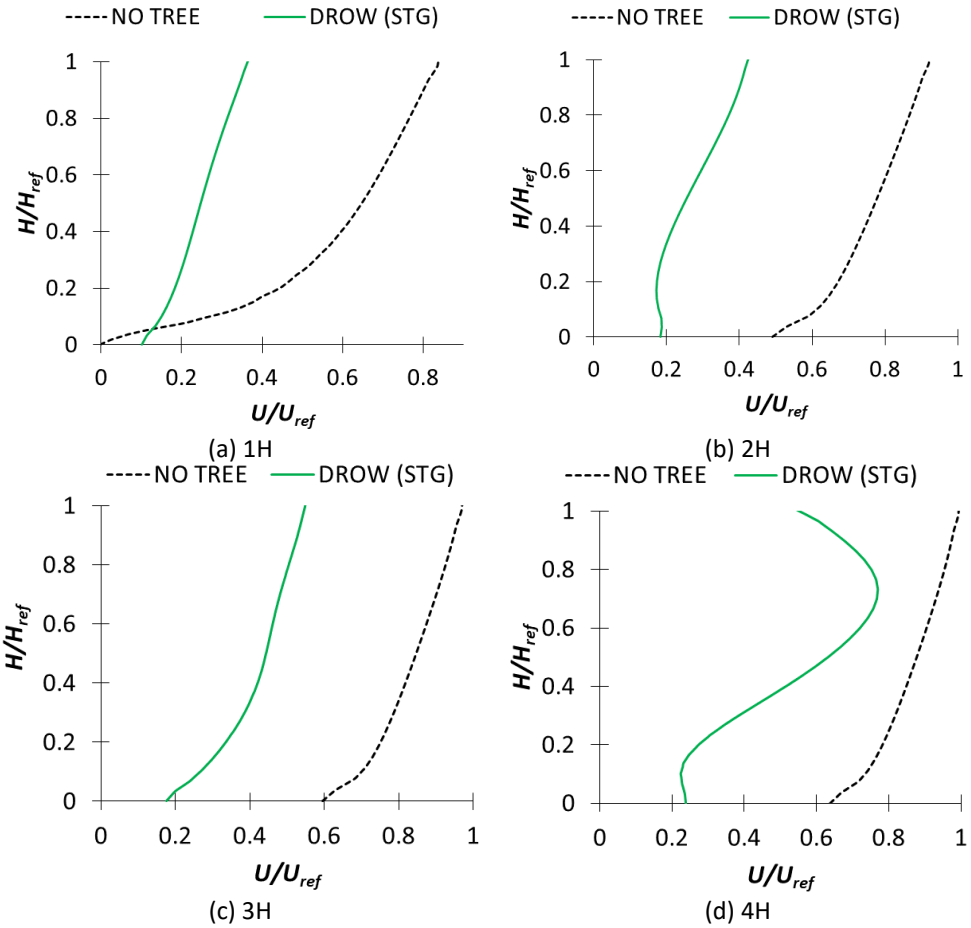

Fig. 19. The vertical U/U_{ref} against H/H_{ref} at the pool section with various distances of (a) 1H, (b) 2H, (c) 3H, and (d) 4H

To identify the turbulence along the pool section, Figure 20 shows the vertical k/U_{ref}^2 against H/H_{ref} with different distances. As displayed, the k/U_{ref}^2 of double rows increased as H/H_{ref} increased for all distances. Meanwhile, at 4H k/U_{ref}^2 for double rows was lowered on the ground with $0.012k/U_{ref}^2$ and it was gradually increased from $0.4H/H_{ref}$ with $0.03k/U_{ref}^2$ onwards. The fluctuation in k/U_{ref}^2 beyond 4H from $0.4H/H_{ref}$ was due to the presence of porous vegetation windbreak as 4H was in bleeding flow characterized as Region C. These windbreaks significantly decrease wind velocity, breaking down larger-scale upwind turbulent eddies, and generating a recirculation zone downwind which increased k/U_{ref}^2 [62,63].

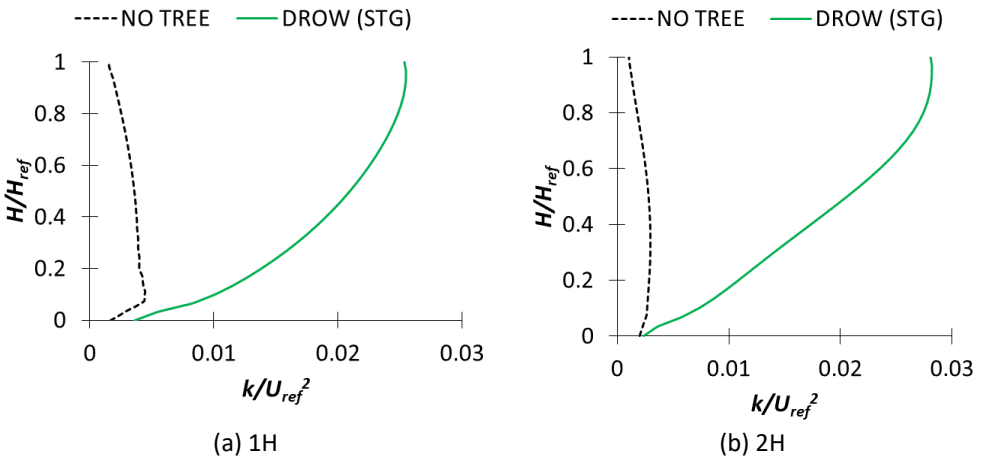

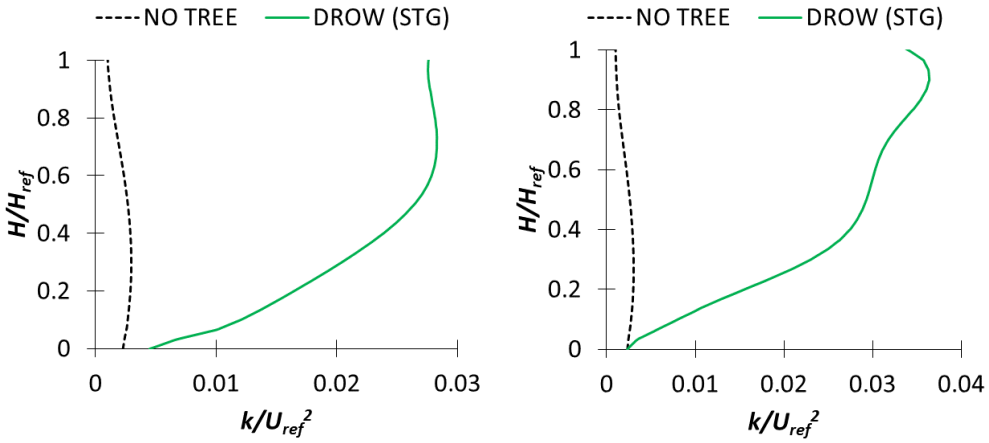

Fig. 20. The vertical k/U_{ref}^2 against H/H_{ref} at the pool section with various distances of (a) 1H, (b) 2H, (c) 3H, and (d) 4H

Figure 21 shows the vertical U/U_{ref} and k/U_{ref}^2 as a function of H/H_t on the leeward side of the windbreak. The leeward side was characterized at three different locations: $0.5H_t$, $1.0H_t$, and $1.5H_t$. This allows for the observation of wind flow characteristics closed to the windbreak. In Figure 21(a) the highest value of U/U_{ref} was observed at the trunk height, specifically at $1.0H_t$, and $1.5H_t$ up to $1.4U/U_{ref}$. As H/H_t gradually increased to the canopy height, U/U_{ref} started to decline and reach $0.2U/U_{ref}$ at all locations. This was due to the CE tree exhibiting a branchless trunk in the area between the bottom of the canopy and the ground. These created a gap through which the oncoming wind would pass, led to channeling flow to satisfy the conservation of mass, and generated higher wind velocity as it flowed through this region [57]. Therefore, a strong turbulence zone was formed as in Figure 21(b) closer to the tree trunks or on the leeward side of CE, which increased in the value of k/U_{ref}^2 at $0.5H_t$ reaching $0.043k/U_{ref}^2$.

Similar results were found in Torshizi *et al.,* [64] which used *Tamarix aphylla* as multiple rows windbreak and the findings demonstrated the windbreak deflections were observed in the profiles across normalized heights, z/h ranging from 0.2 to 0.8 for all distances. This was due to the consistent positive trend observed in windbreak deflections, which aligned with a negative trend in wind velocity as displayed in Figure 21(a) beyond $0.2H/H_t$ indicating the windbreak exerted a drag on the wind flow, resulting in a local decrease in wind velocity as its close to the windbreak's height.

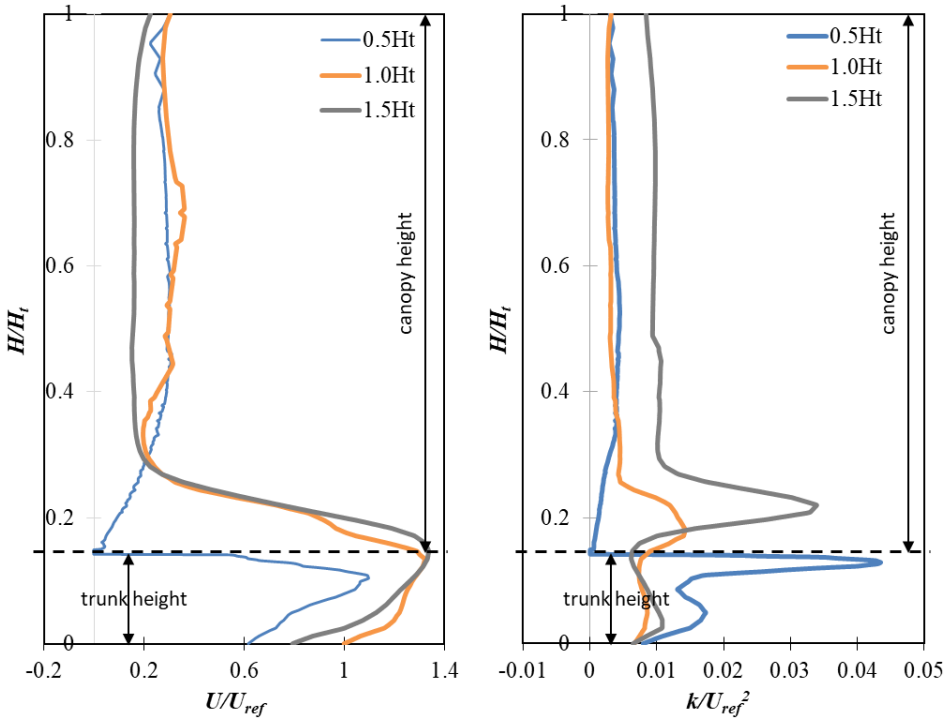

Fig. 21. The vertical (a) U/U_{ref} against H/H_t and (b) k/U_{ref}^2 against H/H_t in the pool section

In terms of wind comfort criteria, Figure 22 shows the joint probability distribution function of a quality class according to the Dutch Standard NEN 8100. The quality classes experienced in the pool section were classes A, B, and C with a P(U_{THR}) value of 9% which was only 1% lower compared to the single-row windbreak (10%). The percentage of the classes for each quality was 46% for class A, 13% for class B, 33% for class C, and 9% for class D. This result was in good agreement with the findings of the previous study indicated that the staggered double rows protected only 61% wind reduction area of the whole domain, while 3% suffered an increase in wind velocity [60]. This was due to venturi effects from the small spacing between trees and rows, in which the wind flow constricted the flow cross-section and created a significant amplification of the velocity between the tree's trunk towards the building. The passages between trees can be responsible for increased wind velocity near ground level which caused wind nuisance for pedestrians due to a converging passage, also called venturi throat [65].

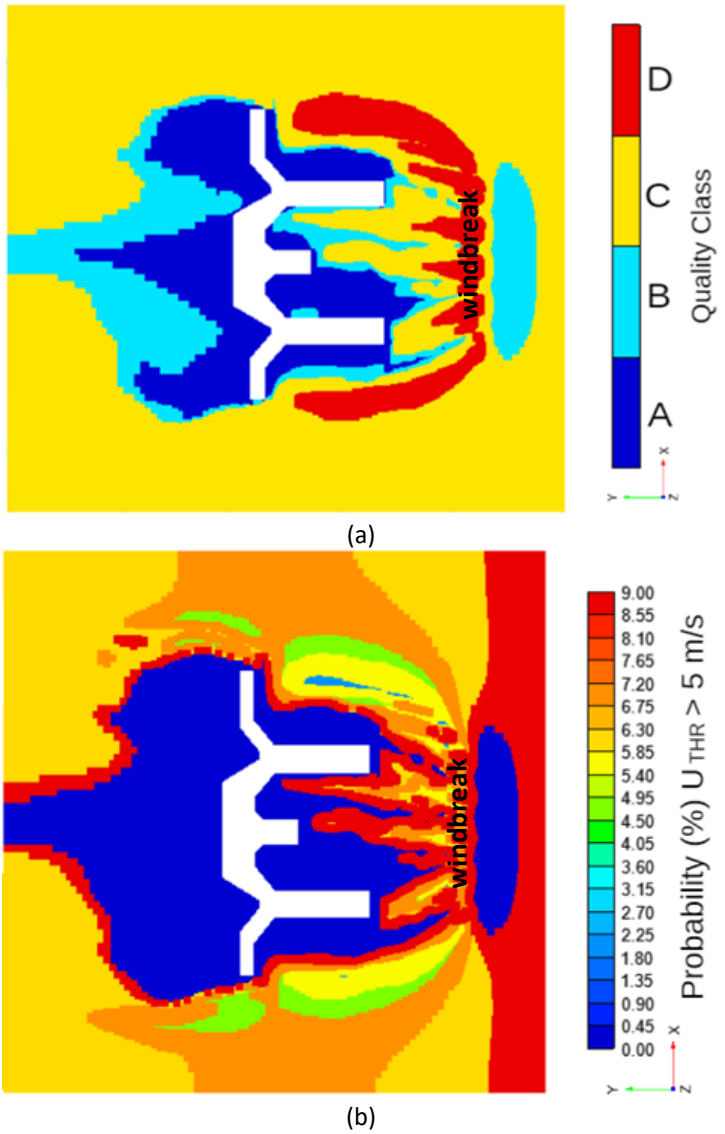

Fig. 22. The joint probability distribution function of (a) quality class according to the Dutch Standard NEN 8100 and (b) exceedance probabilities for wind nuisance for a staggered double rows windbreak tree measured at 1.5 m height

3.4 Linear Double Row Windbreak Simulation

Linear windbreaks were one of the types of windbreak arrangement, which align similarly behind the first-row windbreak. Figure 23 shows a linear double row of trees arrangement in the simulation. The CE tree was aligned parallel to the beach and arranged in a rectangular configuration with a tree spacing of 4 m x 8 m. The tree model in this study had a maximum height of 30 m with a trunk height of 5 m.

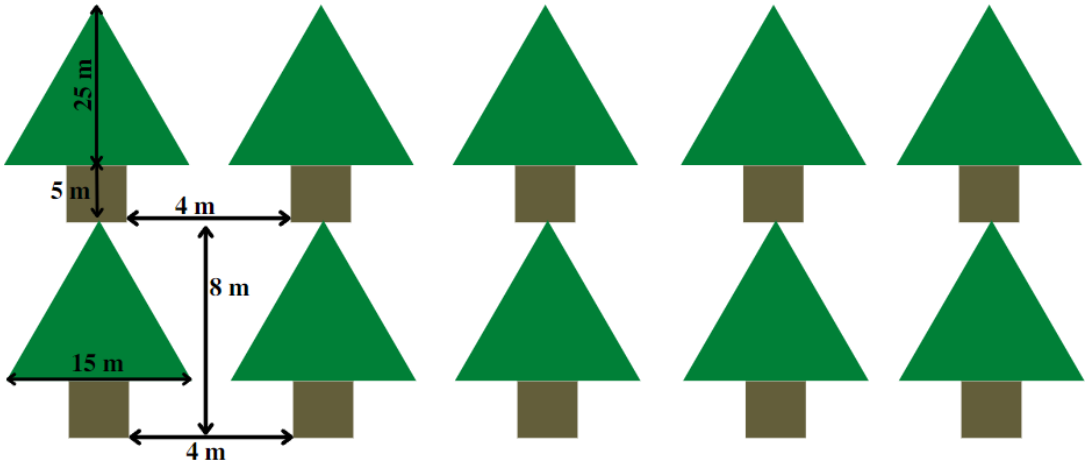

Fig. 23. The canopy distance of a linear double row of CE tree models in the simulation

The arrangement of CE trees from the top view of the building resort were displayed in Figure 24. The distance between the beach line and the first row of trees was 10 m, while each row was spaced 8 m apart from trunk to trunk. To assess the velocity distribution around linear double rows windbreak simulation, Figure 25 shows a two-dimensional wind flow at pedestrian height. In this section, the analysis focused on analyzing the wind flow in front of the building which distance ranging from 1H to 4H, as well as the leeward side of the windbreak from 0.5Ht to 1Ht.

Fig. 24. The view of the building resort and linear double rows windbreak location

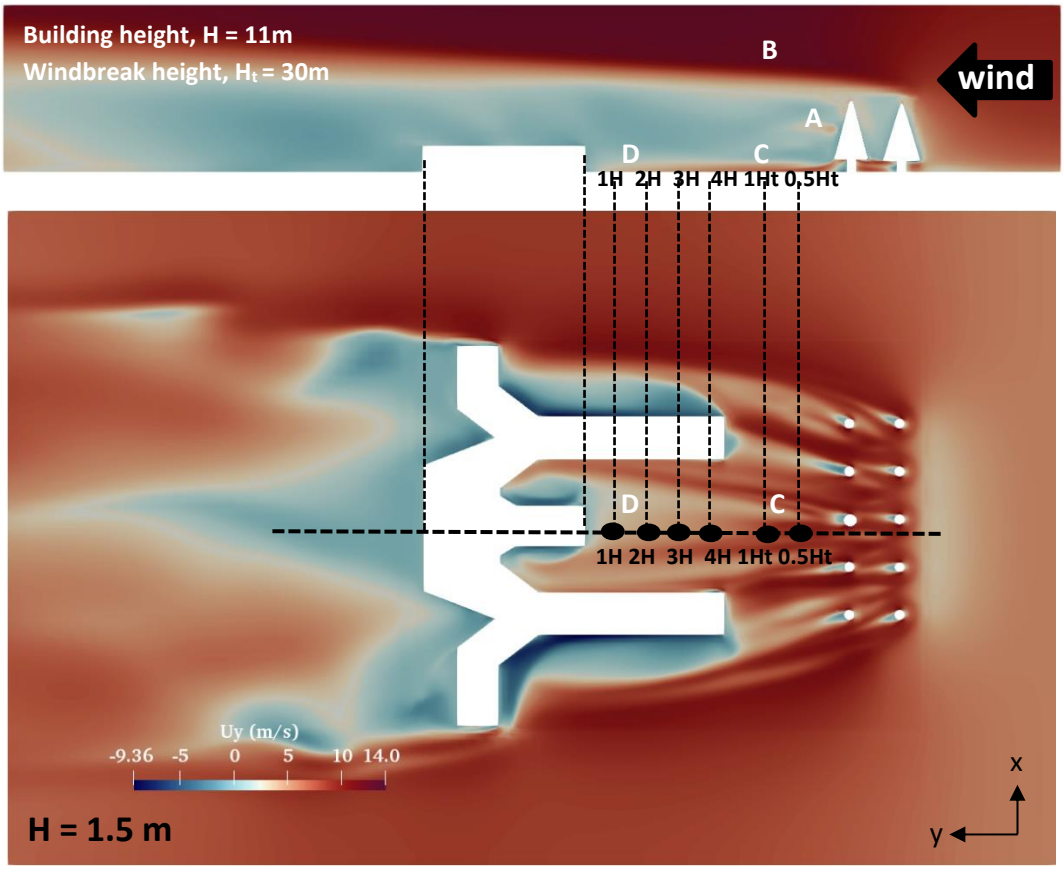

Fig. 25. The velocity distribution of the two-dimensional flow field around the windbreak simulation at 1.5 m height

To evaluate the wind reduction in linear double rows windbreak, Figure 26 shows the relationship between vertical U/U_{ref} against H/H_{ref} at the pool section with different distances. The presence of linear double rows windbreak resulted in a strong deceleration in wind velocity of approximately 70.11% for 1H, 73.88% for 2H, 77.50% for 3H, and 77.91% for 4H. Moreover, as the distance increased from the building wall, the wind reduction exhibited a corresponding increase. The higher percentage of wind reduction was due to the presence of channel effects generated between the spaces between the trees, which facilitated the trapping of wind. Khodayari *et al.,* [56] findings demonstrated that the utilization of a linear double rows planting arrangement was an effective strategy for enhancing the effectiveness of a tree's windbreak in reducing wind velocity. These results were consistent with the wind tunnel simulation by Ma *et al.,* [66] and Yinghua *et al.,* [67], which revealed the effect on the wind velocity varies behind the windbreak region due to the different configurations of the trees and the formation of different airflow field structures.

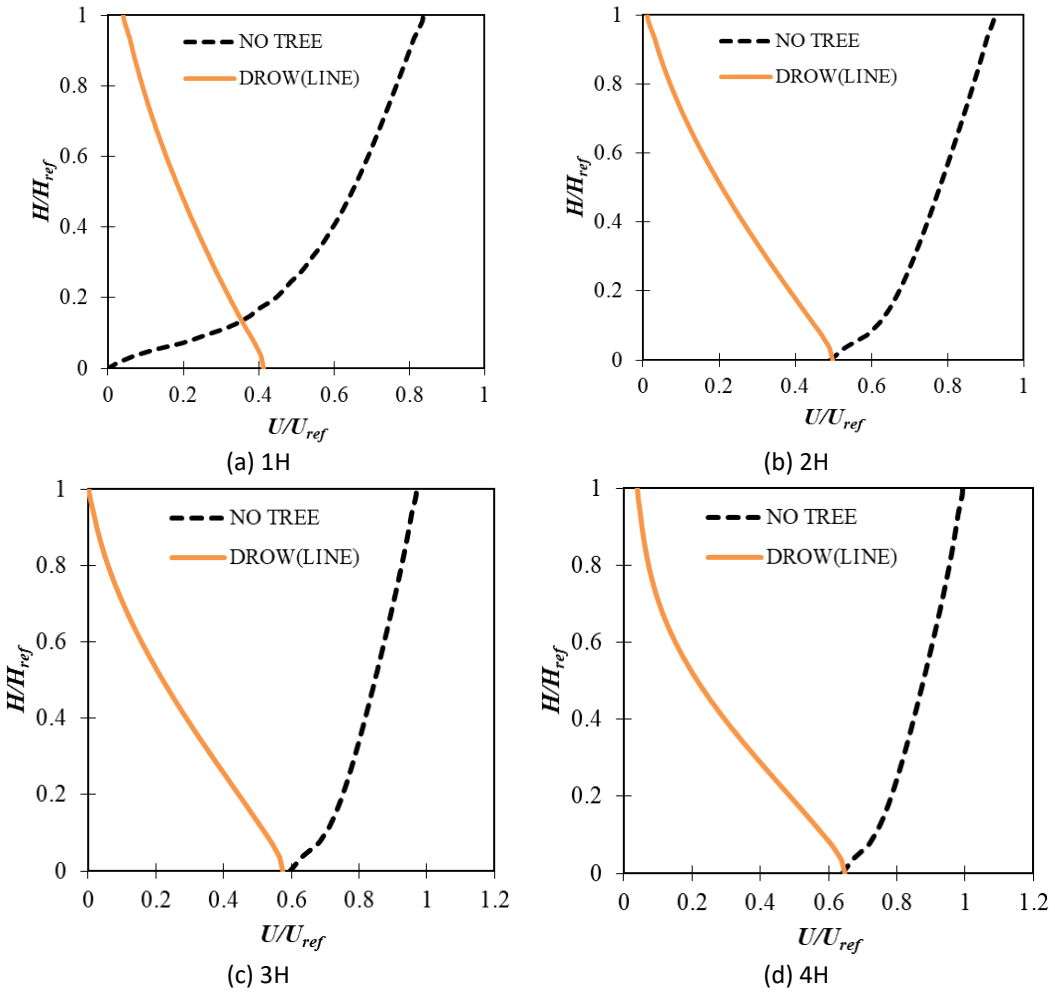

Fig. 26. The vertical U/U_{ref} against H/H_{ref} at the pool section with various distances of (a) 1H, (b) 2H, (c) 3H, and (d) 4H

Figure 27 shows the vertical k/U_{ref}^2 as a function of H/H_t on the windward side of the building. The percentage difference in the increased of k/U_{ref}^2 between linear double rows and no tree was as follows: 52.97% at 1H, 66.75% at 2H, 68.43% at 3H, and 63.03% at 4H. The location specifically at 2H and 3H characterized by the highest increment of k/U_{ref}^2 exhibits the strongest turbulence energy originating from the mixing zone formed by the windbreak which was located within the quiet zone of region D [68]. These results indicated that the presence of linear double rows windbreaks played a beneficial role in mitigating the impact of strong winds and providing wind comfort to the pedestrian.

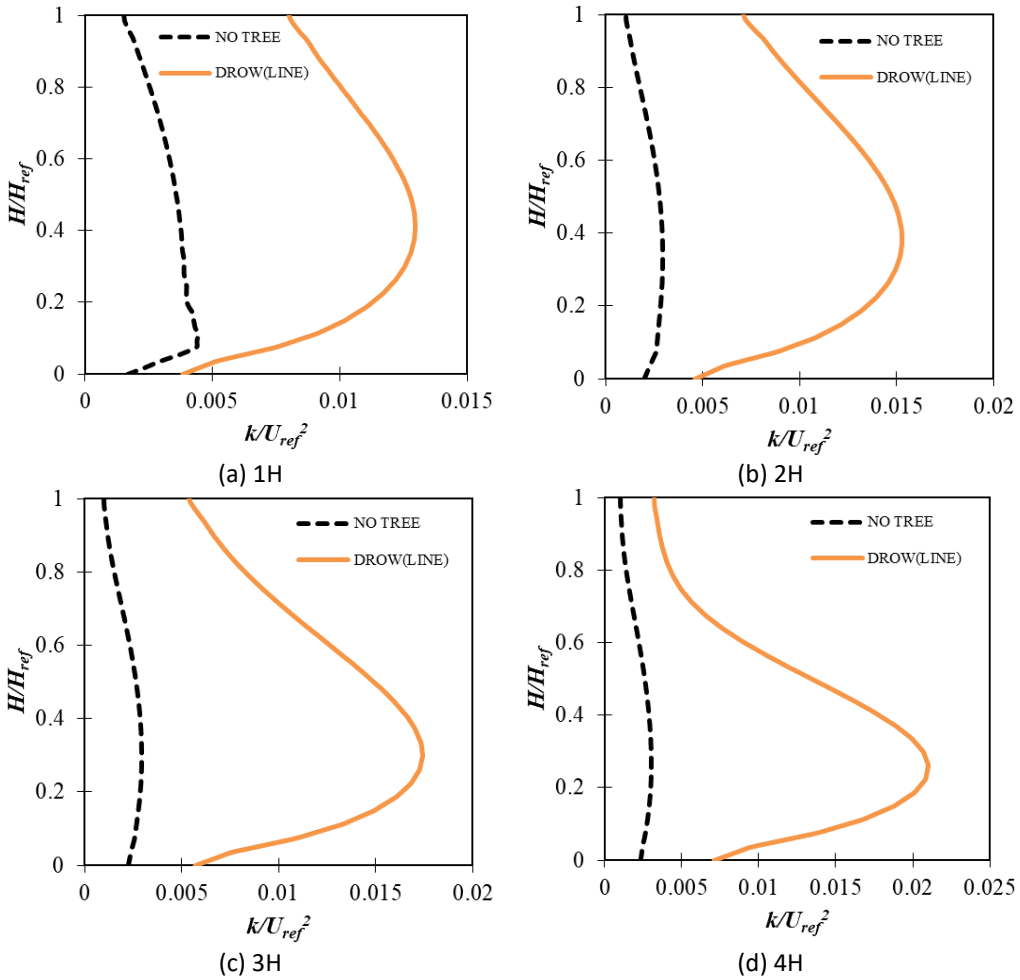

Fig. 27. The vertical k/U_{ref}^2 against H/H_{ref} at the pool section with various distances of (a) 1H, (b) 2H, (c) 3H, and (d) 4H

Figure 28 shows the vertical U/U_{ref} and k/U_{ref}^2 as a function of H/H_t on the leeward side of the windbreak. The leeward side was characterized at three different locations: $0.5H_t$, $1.0H_t$, and $1.5H_t$. This allows for the observation of wind flow characteristics closed to the windbreak. In Figure 28(b), high k/U_{ref}^2 was observed at 1.0Ht and 1.5Ht from $0.05H/H_t$ to $0.6H/H_t$ due to the greater degree of wind velocity fluctuation and more intensive mixing of a large part of wind flow (known as bleeding flow lies in Region C still penetrated the canopy with its velocity gradually reduced by the porous media.

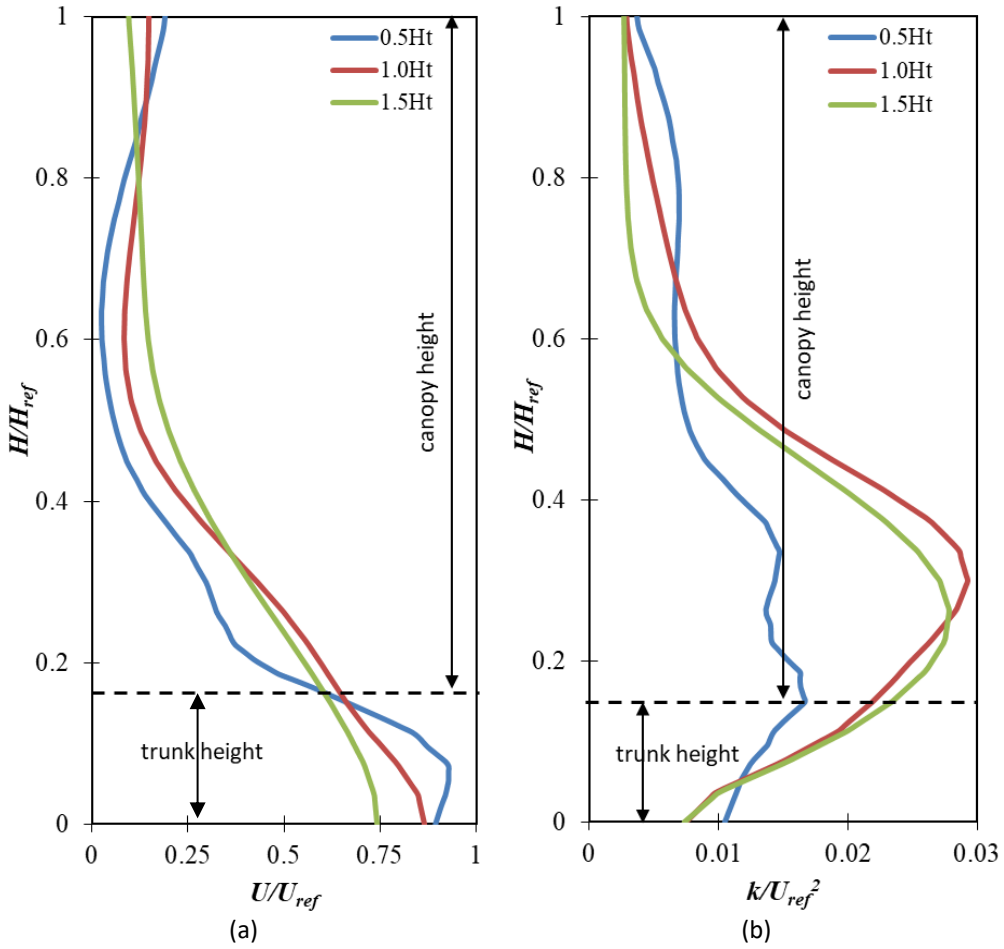

Fig. 28. The vertical (a) U/U_{ref} against H/H_t and (b) k/U_{ref}^2 against H/H_t in the pool section

Figure 29 depicted the joint probability distribution function of a quality class and its exceedance probabilities of a particular wind comfort, defined by the Dutch Standard NEN 8100. The quality class in Figure 29(a) displayed the quality class of B and C in the pool section, which was categorized as a moderate level for strolling and a poor level for sitting in that area. However, the P(U_{THR}) presented in Figure 29(b) showed that the pool section experienced the highest P(U_{THR}) value, with the probability of threshold wind velocity exceeding 5 m/s by approximately 12%. The P(U_{THR}) for linear windbreak in the pool section was recorded as highest among the arrangement of the other windbreak, which was staggered double rows were maximum P(U_{THR})=9% and single-row windbreak was maximum P(U_{THR})=10%. The percentage of the classes for each quality was 41% for class A, 11% for class B, 42% for class C, and 5% for class D. In the linear windbreak arrangement, the trees in the second row were in the sheltered zones from the first-row tree. The sheltered zone merged to form two larger protected zones. However, due to the column spaces being small (4 m, which was 0.27 times of canopy width of 15 m), higher velocity "streets" were formed between each column of windbreak as shown in orange color in Figure 29(b). Similar results were found in field observations from Okin *et al.,* [69], wind tunnel experiments from Burri *et al.,* [70], and simulations from Dupont *et al.,* [71].

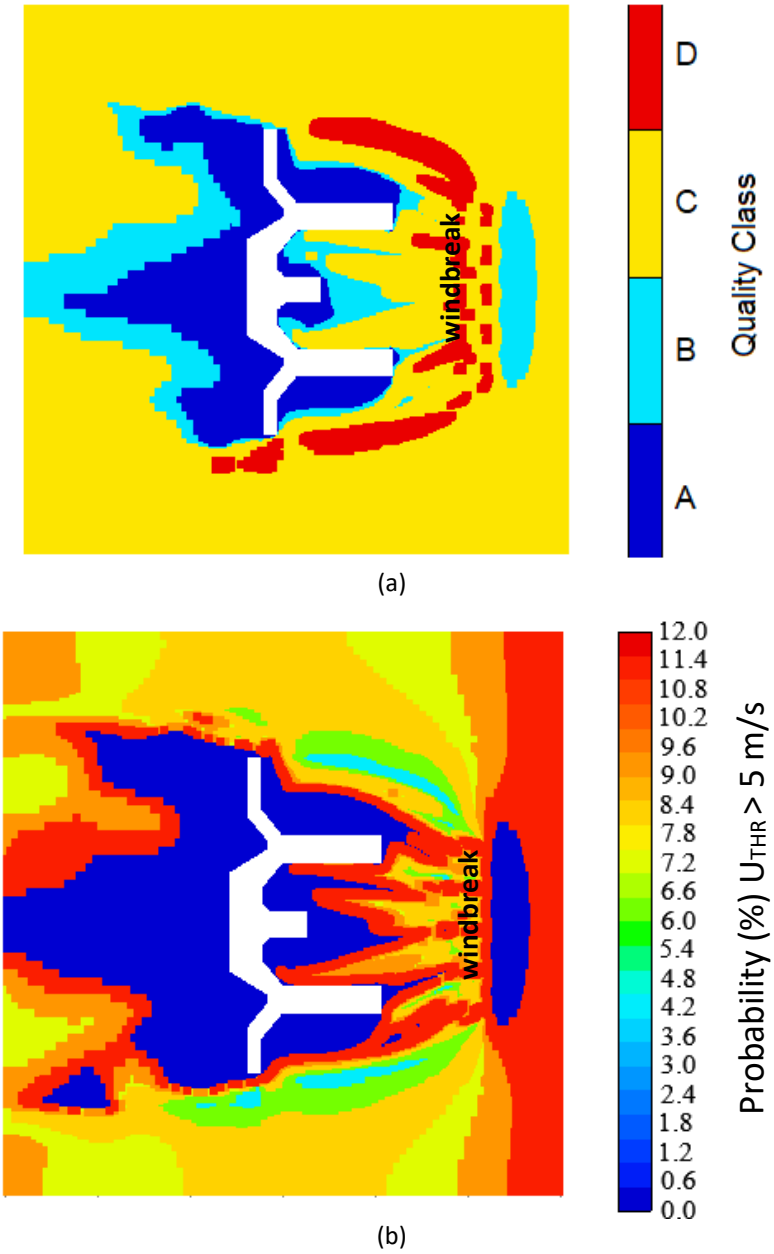

Fig. 29. The joint probability distribution function of (a) quality class according to the Dutch Standard NEN 8100 and (b) exceedance probabilities for wind nuisance for a linear double rows' windbreak tree measured at 1.5 m height

3.5 Design a Better Windbreak

The main purpose of learning the flow field around single and double rows trees is to design a more efficient and effective windbreak nearby the coastal area. To better evaluate the protection efficiency of the tree could be determined by the characteristics of each tree and its distribution. In this study, the single row was studied with a linear and staggered double rows arrangement of the simulated canopies. Figure 30 shows flow regimes behind a windbreak barrier. Generally, as the wind approaches a windbreak, the pressure in front of the canopy increases. This blockage effect results in a crossflow perpendicular to the wind direction, which causes a marginal increase in surface wind velocity near the windbreak called the displacement flow in regime I (called Region B). However, a

significant part of wind referred to as bleeding flow in regime II (called Region C) continues to penetrate the canopy as its velocity is gradually reduced by the presence of porous media. Subsequently, a region characterized by lower surface wind velocity which is known as a quiet zone lies within flow regime III (called Region D) [53].

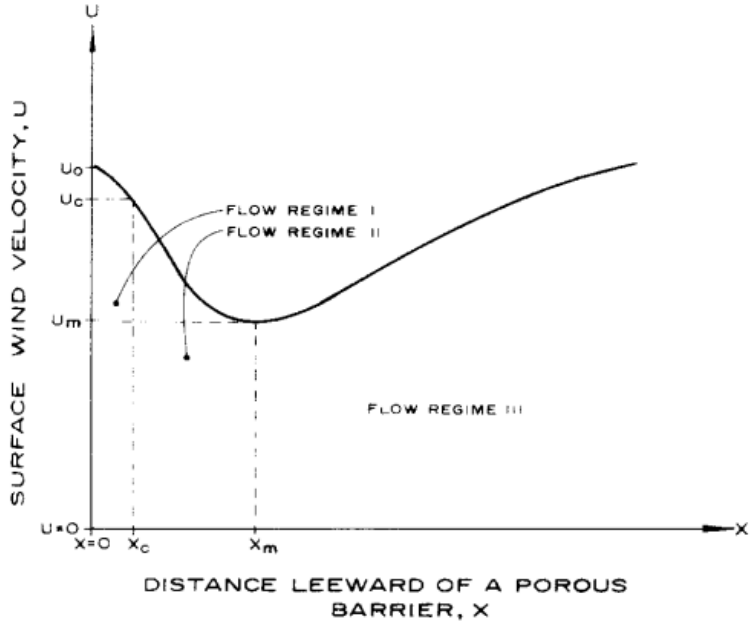

Fig. 30. The three flow regimes behind a windbreak barrier [72]

Figure 31 depicted the wind velocity for different arrangements at various distances from the ground. As seen, wind velocity undergoes a sudden decrease after passing through the windbreak at x/H = 11, because of the relative stagnation condition created behind the windbreak. As the wind got away from the windbreak, the velocity decreased again, and nearby buildings due to its standing vortex. It was obvious that the wind vortex affected not only the flow near the building but also the entire flow field between the building and the windbreak, especially at Region C and Region D. To determine an optimal design for windbreaks, it is essential to conduct a reasonable evaluation of the windbreak effect.

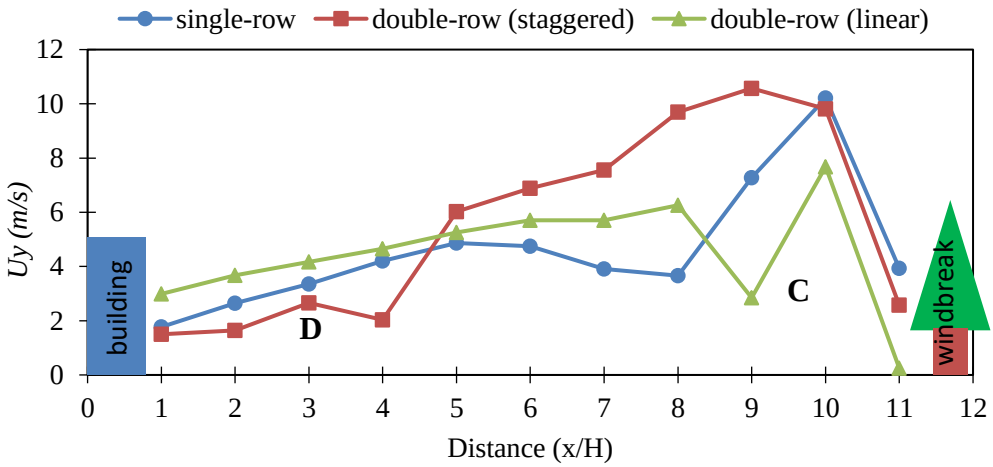

Fig. 31. The windbreak arrangements of the incoming wind velocity, *Uy* at a height of 1.5 m from the ground

In the simulation, the shelter effect was primarily influenced by the windbreak distance and velocity reduction. Therefore, the evaluation of the windbreak distance in this study was conducted using the barrier effective index, *BEI* [73]. The calculation of *BEI* depends on the selection of the leeward distance from the windbreak. In this study, distances from 1H, 2H, 3H, and 4H were selected for further evaluation to calculate the shelter distance for different row arrangements. Table 4 shows the *BEI* calculated for single and double rows with different types of arrangements with different distances from the windbreak. Based on the calculated *mBEI*, staggered double rows showed the highest value of approximately 1.92, compared to both linear double rows and single-row windbreak. The highest value of *mBEI* indicated a greater downwind shelter distance of the windbreak. Therefore, staggered double rows are the best option when considering mainly the shelter effect extent behind the windbreak. The finding was aligned with a study by Guo *et al.,* [20], in which the *mBEI* of staggered rows of *Artemisia* and *Salix* windbreaks was greater than aligned rows regardless of incoming velocity, which indicates the staggered rows exhibit an optimal shelter effect.

Table 4
The calculated *BEI* for different windbreak arrangements

Arrangement	*BEI* (1H)	*BEI* (2H)	*BEI* (3H)	*BEI* (4H)	*mBEI*
Single row	0.82	1.43	1.91	2.21	1.59
Double row (staggered)	0.84	1.65	2.11	3.08	1.92
Double row (linear)	0.65	1.15	1.52	1.80	1.28

To evaluate the shelter effect of windbreak arrangement, Figure 32 shows the different windbreak arrangements under the incoming velocity of U_{ref} = 8.46 m/s, of 1.5 m from the ground. At a leeward distance (≤4H) from the windbreaks nearby the building, staggered double rows displayed the highest *mRc* among the other types of arrangement, which indicated the best shelter effect; conversely, the linear double rows had an even lower *mRc* than the single row arrangement. Additionally, at a leeward distance (≥8H), the linear double rows of *mRc* were larger than the other arrangements, due to its *BEI* value of 6.5 in Figure 32(b), which indicated that it has a longer shelter distance compared to the others. Therefore, the staggered double rows are most effective in reducing near-surface wind velocity, while linear double rows offer the optimal shelter distance. These results were in line with Liu *et al.,* [60], which showed that the staggered arrangement provided the greatest protection, approximately 75% of the area.

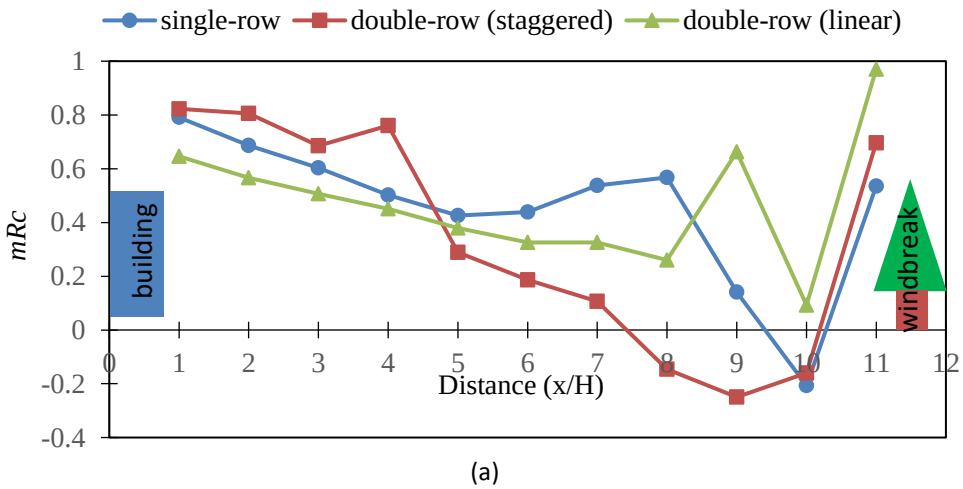

(a)

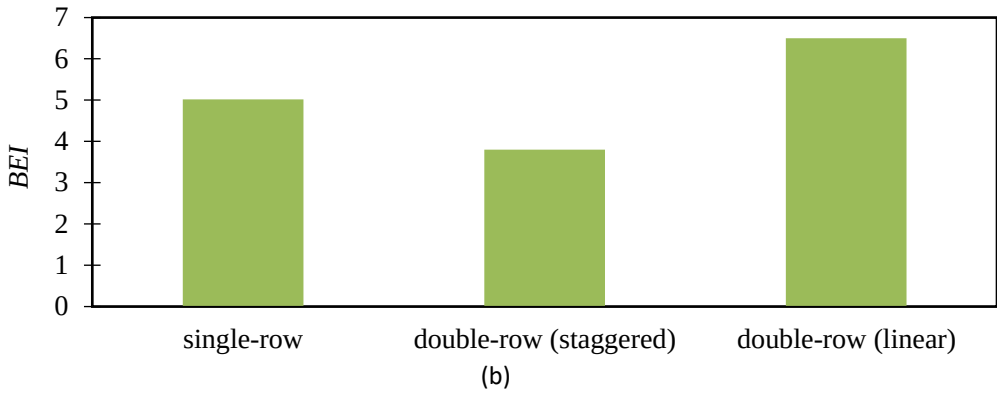

(b)

Fig. 32. The windbreak arrangements of the (a) shelter effect under an incoming velocity of U_{ref} = 8.46 m/s, and (b) *BEI* for different rows

Table 5 shows the total percentage of quality classes in wind comfort with different rows arrangement. The quality class for Classes A and B showed a significant percentage for all rows arrangement. The table demonstrates that planting vegetative windbreaks improved the wind quality in the building resort, which enhanced comfort to pedestrians for all types of outdoor and leisure activities. However, for Class C and Class D, staggered double rows indicate lower percentages which are 20.4% and 0.7%, compared with other arrangements. Therefore, the staggered double rows arrangement may be more suitable for achieving optimum levels of wind comfort around building resorts for open coast areas.

Table 5
The total percentage of quality classes of different rows arrangement

Arrangement	Quality Class (%)			
	A	B	C	D
Single-row	46.2	12.4	38.5	2.9
Staggered double-row	52.3	26.6	20.4	0.7
Linear double-row	41.3	11.3	42.4	5.4

The main contributions of this study can be summarized as follows. First, the windbreak model was replicate the realistic conical shape of a CE tree, which was then applied in the numerical models, to simulate the flow dynamics around the windbreak. This allowed for a comprehensive understanding of the complex interactions between vegetation and the surrounding airflow. Second, the staggered double rows arrangements were identified which is an effective method for determining the optimum arrangement that yielded the best results in terms of sheltering effect. Third, our investigation of different types of rows arrangement overcomes the limitations of wind velocity reduction at the leeward zone especially in open-building resorts that face the coast. Finally, the assessment is to determine the optimum shelter effect and to design a better windbreak, to provide a comfortable and pleasant environment for tourists, particularly in open resorts near the coasts in Southeast Asia. This research emphasizes open coastal resorts, and the consideration of tropical storms further contributes to the novelty of the research. In summary, the simulation of a realistic windbreak model, determining optimal arrangements, overcoming limitations, and consideration of specific environmental factor, adds novelty to the study and expand the knowledge of windbreaks design.

4. Conclusions

Based on the CFD simulation of airflow across single and double rows, CFD simulation with the RNG *k-ε* turbulence closure scheme provides good predictions of the airflow field for both single and double rows. The current study numerically investigated the wind comfort in the leisure area around the building resort, on the different arrangement of rows to evaluate the ability of the natural windbreak of *Casuarina equisetifolia* for reducing wind velocity at different distances behind the windbreak. The significant outcomes based on the research objectives are as follows

i. As observed, the assessment of wind conditions around the building, and the comfort of pedestrians was specifically focused on the pool area, which serves as a public recreational zone. The wind velocity at the windward side of the building changed drastically in the pool section which had negative wind velocity until the wind was near the windward side of the building, where a local peak occurred due to the small vortex region generated in front of the building and near the ground. This vortex was caused by a downward deflection of the flow across the front of the building to the ground, where it deflected again, resulting in a near-bed flow in the opposite direction of the incoming wind direction.
ii. Moreover, for the wind comfort assessment, the map with wind classes at pedestrian level in current condition shows rather large areas with quality class C that indicate up to 27% of probability (U_{THR}>5 m/s) around the building. These areas have a good wind climate for traversing, moderate wind climate for strolling, and poor for sitting. Since the building resort is a place for leisure and tourists spot, it is typically a place for strolling and sitting; thus, steps should be taken to improve the wind condition in these areas, so that it is at least good for strolling and sitting as in Class A or B.
iii. A single row reduces the velocity increased as the distance from the building increases. To assess the accuracy of the results, the relative standard deviation was calculated to calculate the average reduction of U/U_{ref} at the pedestrian height for various locations. The average reduction of U/U_{ref} at each location, are as follows; 1H = 53.18%, 2H = 55.94%, 3H = 57.78%, and 4H = 59.89%. About more than 50% reduction of U/U_{ref} for single row windbreak occurred due to a large scale of wind approached from displacement flow (Region B) which causes a marginal increase o velocity lateral to the tree.
iv. Moreover, in staggered double rows, the wind reduction based on the relative standard deviation of staggered double rows and without windbreak at the pool section at 1H, 2H, 3H, and 4H were determined to be 48.14%, 49.06%, 47.82%, and 46.56%, respectively. The lowest wind reduction at 4H from 0.6H/H_{ref} to 0.8H/H_{ref} was due to the presence of the trees, where oscillations in airflow occurred. These oscillations were caused by increased fluid entropy in the wake and within the trunk [61]. The presence of linear double rows windbreak resulted in a strong deceleration in wind velocity of approximately 70.11% for 1H, 73.88% for 2H, 77.50% for 3H, and 77.91% for 4H. As the distance increased from the building wall, the wind reduction exhibited a corresponding increase. The higher percentage of wind reduction was due to the presence of channel effects generated between the spaces between the trees, which facilitated the trapping of wind.
v. From the research findings, staggered double rows display the highest *mRc* among the other types of arrangement, which indicates the best shelter effect; conversely, the linear double rows had an even lower *mRc* than the single row arrangement. Additionally, at a leeward distance (≥8H), the linear double rows of *mRc* were larger than the other arrangements, due to its *BEI* value of 6.5, which indicates that it has a longer shelter distance compared to the others. Therefore, the staggered double rows are most effective in reducing near-surface

wind velocity, while linear double rows offer the optimal shelter distance. These results were in line with Liu *et al.,* [60], which showed that the staggered arrangement provided the greatest protection, approximately 75% of the area.

vi. Besides, the vegetative windbreaks improved the wind quality around the building resort, which enhanced comfort for pedestrians for all types of outdoor and leisure activities. However, staggered double rows indicate lower percentages, specifically 20.4% and 0.7%, for Class C and Class D, respectively when compared with other row arrangements. Therefore, the staggered double rows arrangement may be a more suitable option for achieving optimum levels of wind comfort around building resorts located in the open coastal areas. The improvement of wind velocity played an important role in enhancing overall wind comfort and safety during various outdoor and leisure activities in the building resort. By strategically planting windbreaks, the resort management ensured that their guests could enjoy their activities without being experienced uncomfortable or strong winds, thereby creating a more pleasant environment around the building area.

Finally, this study offers to provide guidelines to resort developers with a set of best practices that consider both the aesthetics environment and wind comfort to the pedestrians. By following these approaches, developers can decide when to select the most suitable and optimal rows arrangement and windbreak design for their building resort. Besides, the specific challenges can be addressed in the guideline, which is faced by open coast resorts, where wind conditions may be extreme. In such cases, the staggered double rows arrangement, despite its lower percentages for certain quality classes, may be recommended as an option due to its potential to mitigate the impact of strong winds or storms and maintain a comfortable environment for pedestrians and resort guests. In summary, comprehensive guidelines can be beneficial in standardizing the approach towards wind comfort around building resorts. These guidelines can serve as effective resources for developers in decision-making concerning row arrangements, windbreak design for open coast buildings, and identifying suitable approaches to optimize wind comfort while preserving the overall aesthetic nature of the resort.

Acknowledgement

The authors would like to thank Universiti Teknologi Malaysia for supporting this research through the Transdisciplinary Research Grant (Vote 06G99). The authors would also like to express their gratitude to the Malaysian Meteorological Department, Holiday Villa Beach Resort & Spa Langkawi, Wind Tunnel Laboratory Malaysia-Japan International Institute of Technology (MJIIT), and Langkawi Development Authority (LADA) for supporting this research.

References

[1] Ministry of Tourism, Arts and Culture Malaysia. "Tourist Arrivals." *MyTourismData*.
[2] Mustapha, Mazlina, and Khairil Wahidin Awang. "Sustainability of a beach resort: A case study." *International Journal of Engineering & Technology* 7, no. 2.29 (2018): 210-214. https://doi.org/10.14419/ijet.v7i2.29.13319
[3] The Star Online. "Resort Chalets in Terengganu halts operations following monsoon season." *The Star Online*. October 4, 2016.
[4] Smith, Russell Arthur. "Beach resorts: A model of development evolution." *Landscape and Urban Planning* 21, no. 3 (1991): 189-210. https://doi.org/10.1016/0169-2046(91)90018-H
[5] Senapati, Sibananda, and Vijaya Gupta. "Socio-economic vulnerability due to climate change: Deriving indicators for fishing communities in Mumbai." *Marine Policy* 76 (2017): 90-97. https://doi.org/10.1016/j.marpol.2016.11.023
[6] Beriatos, Elias. "Uncontrolled urbanization, tourism development and landscape transformation in Greece." In *Proceedings of 44th ISOCARP Congress.* 2008.

[7] Omar, Shida Irwana, Abdul Ghapar Othman, and Badaruddin Mohamed. "The tourism life cycle: An overview of Langkawi Island, Malaysia." *International Journal of Culture, Tourism and Hospitality Research* 8, no. 3 (2014): 272-289. https://doi.org/10.1108/IJCTHR-09-2013-0069
[8] Nambiar, Predeep. "Langkawi's 99 reclaimed islands project on track, says Sanusi." *Free Malaysia Today*. September 23, 2021.
[9] Mohamed, Juliana, and Muhammad Rizal Razman. "Management and Initiatives Towards Sustainable Coastal Development in Malaysia: Experience from Reclamation Activities in Malacca (Pengurusan dan Inisiatif ke Arah Kelestarian Pembangunan Kawasan Pinggir Pantai di Malaysia: Dari Pengalaman Aktiviti Penambakan di Melaka)." *Asian Journal of Environment, History and Heritage* 2, no. 2 (2018).
[10] Valuation and Property Services Department. "Leisure Property Stock Table Q4 2022." *Malaysia Ministry of Finance*.
[11] Hassan, Ahmad Sanusi, Aymen Emalgalfta, and Ku Azhar Ku Hassan. "Development of Successful Resort Design with Vernacular Style in Langkawi, Malaysia." *Asian Culture and History* 2, no. 1 (2010): 85. https://doi.org/10.5539/ach.v2n1p85
[12] Jaafar, Mastura, S. Mostafa Rasoolimanesh, and Safura Ismail. "Perceived sociocultural impacts of tourism and community participation: A case study of Langkawi Island." *Tourism and Hospitality Research* 17, no. 2 (2017): 123-134. https://doi.org/10.1177/1467358415610373
[13] Langkawi Municipal Council. "Rancangan Tempatan Daerah Langkawi 2001-2015 (Langkawi District Local Plan 2001-2015)." *Langkawi Municipal Council*, 2005.
[14] Bernama. "Met Malaysia issues bad weather warning in several states." *Malaysia Kini*. June 18, 2018.
[15] Malaysia Meteorological Department. "Laporan Tahunan Annual Report MET Malaysia." *Malaysia Meteorological Department*, 2019.
[16] Bernama. "Storm damages 17 houses, 15 cars in Langkawi." *Free Malaysia Today*. November 7, 2020.
[17] Brandle, James R., Laurie Hodges, and Xinhua H. Zhou. "Windbreaks in North American agricultural systems." In *New Vistas in Agroforestry: A Compendium for 1st World Congress of Agroforestry*, 2004, pp. 65-78. Springer Netherlands, 2004. https://doi.org/10.1007/978-94-017-2424-1_5
[18] Zhou, X. H., J. R. Brandle, C. W. Mize, and E. S. Takle. "Three-dimensional aerodynamic structure of a tree shelterbelt: Definition, characterization and working models." *Agroforestry Systems* 63 (2005): 133-147. https://doi.org/10.1007/s10457-004-3147-5
[19] Bitog, J. P., I-B. Lee, H-S. Hwang, M-H. Shin, S-W. Hong, I-H. Seo, E. Mostafa, and Z. Pang. "A wind tunnel study on aerodynamic porosity and windbreak drag." *Forest Science and Technology* 7, no. 1 (2011): 8-16. https://doi.org/10.1080/21580103.2011.559939
[20] Guo, Zhiyi, Xiaofan Yang, Xiaoxu Wu, Xueyong Zou, Chunlai Zhang, Hui Fang, and Hongxu Xiang. "Optimal design for vegetative windbreaks using 3D numerical simulations." *Agricultural and Forest Meteorology* 298 (2021): 108290. https://doi.org/10.1016/j.agrformet.2020.108290
[21] Heisler, Gordon M., and David R. Dewalle. "2. Effects of windbreak structure on wind flow." *Agriculture, Ecosystems & Environment* 22 (1988): 41-69. https://doi.org/10.1016/0167-8809(88)90007-2
[22] Jiao-jun, Zhu, Liu Zu-gen, Li Xiu-fen, Takeshi Matsuzaki, and Yutaka Gonda. "Review: effects of wind on trees." *Journal of Forestry Research* 15, no. 2 (2004): 153-160. https://doi.org/10.1007/BF02856753
[23] Mehranian, Hamed, and Azizan Marzuki. "Beach users' perceptions toward beach quality and crowding: A case of Cenang Beach, Langkawi Island, Malaysia." *Sea Level Rise and Coastal Infrastructure* (2018): 181-196. https://doi.org/10.5772/intechopen.76614
[24] Tripadvisor. "Photo: Holiday Villa Langkawi." *TripAdvisor LLC*, 2022.
[25] Tominaga, Yoshihide, Akashi Mochida, Ryuichiro Yoshie, Hiroto Kataoka, Tsuyoshi Nozu, Masaru Yoshikawa, and Taichi Shirasawa. "AIJ guidelines for practical applications of CFD to pedestrian wind environment around buildings." *Journal of Wind Engineering and Industrial Aerodynamics* 96, no. 10-11 (2008): 1749-1761. https://doi.org/10.1016/j.jweia.2008.02.058
[26] Foale, Mike. *Coconut Odyssey: The Bounteous possibilities of the tree of life*. Australian Centre for International Agricultural Research, 2003.
[27] Parnell, J., and P. Chantaranothai. "Myrtaceae." *Flora of Thailand* 7, no. 4 (2002): 778.
[28] Corner, Edred John Henry. *Wayside trees of Malaya in two volumes*. No. Ed. 3. Malayan Nature Society, 1988.
[29] Soepadmo, E., L. G. Saw, R. C. K. Chung, and R. Kiew. *Tree Flora of Sabah and Sarawak*. Sabah Forestry Department, Forest Research Institute Malaysia (FRIM), Sarawak Forestry Department, 2011.
[30] Whistler, W. Arthur, and Craig R. Elevitch. "Syzygium malaccense (Malay apple)." *Species Profiles for Pacific Island Agroforestry*, 2006.
[31] Yakhot, V., S. A. Orszag, S. Thangam, T. B. Gatski, and C. G. Speziale. "Development of turbulence models for shear flows by a double expansion technique." *Physics of Fluids A: Fluid Dynamics* 4, no. 7 (1992): 1510-1520. https://doi.org/10.1063/1.858424

[32] Ries, Kai, and Joachim Eichhorn. "Simulation of effects of vegetation on the dispersion of pollutants in street canyons." *Meteorologische Zeitschrift-Berlin* 10, no. 4 (2001): 229-234. https://doi.org/10.1127/0941-2948/2001/0010-0229
[33] Balczó, Márton, Christof Gromke, and Bodo Ruck. "Numerical modeling of flow and pollutant dispersion in street canyons with tree planting." *Meteorologische Zeitschrift* 18, no. 2 (2009): 197. https://doi.org/10.1127/0941-2948/2009/0361
[34] Kang, Geon, Jae-Jin Kim, Dong-Ju Kim, Wonsik Choi, and Soo-Jin Park. "Development of a computational fluid dynamics model with tree drag parameterizations: Application to pedestrian wind comfort in an urban area." *Building and Environment* 124 (2017): 209-218. https://doi.org/10.1016/j.buildenv.2017.08.008
[35] Bauer, Lucas. "Winds on the Beaufort scale." *Wind Turbine Models*.
[36] Pourteimouri, Paran, Geert H. P. Campmans, Kathelijne M. Wijnberg, and Suzanne J. M. H. Hulscher. "A numerical study on the impact of building dimensions on airflow patterns and bed morphology around buildings at the beach." *Journal of Marine Science and Engineering* 10, no. 1 (2021): 13. https://doi.org/10.3390/jmse10010013
[37] Patankar, Suhas. *Numerical heat transfer and fluid flow*. Taylor & Francis, 2018. https://doi.org/10.1201/9781482234213
[38] Franke, Jörg, Antti Hellsten, Heinke Schlünzen, and Bertrand Carissimo. "Best practice guideline for the CFD simulation of flows in the urban environment." *PhD diss., COST European Cooperation in Science and Technology*, 2007.
[39] Sisterson, Douglas L., and Paul Frenzen. "Nocturnal boundary-layer wind maxima and the problem of wind power assessment." *Environmental Science & Technology* 12, no. 2 (1978): 218-221. https://doi.org/10.1021/es60138a014
[40] Dwyer Instruments. "Air Velocity Measurement." *Dwyer Instruments*.
[41] Delgado, A., C. Gertig, E. Blesa, A. Loza, C. Hidalgo, and R. Ron. "Evaluation of the variability of wind speed at different heights and its impact on the receiver efficiency of central receiver systems." In *AIP Conference Proceedings*, vol. 1734, no. 1. AIP Publishing, 2016. https://doi.org/10.1063/1.4949063
[42] Ro, K. S., and P. G. Hunt. "Characteristic wind speed distributions and reliability of the logarithmic wind profile." *Journal of Environmental Engineering* 133, no. 3 (2007): 313-318. https://doi.org/10.1061/(ASCE)0733-9372(2007)133:3(313)
[43] Horikawa, Kiyoshi, Shintaro Hotta, and Nicholas C. Kraus. "Literature review of sand transport by wind on a dry sand surface." *Coastal Engineering* 9, no. 6 (1986): 503-526. https://doi.org/10.1016/0378-3839(86)90001-3
[44] Jian, Zhang, Li Bo, and Wang Mingyue. "Study on windbreak performance of tree canopy by numerical simulation method." *The Journal of Computational Multiphase Flows*, vol. 10, no. 4 (2018): 259-265. https://doi.org/10.1177/1757482x18791901
[45] Versteeg, Henk Kaarle, and Weeratunge Malalasekera. *An introduction to computational fluid dynamics: the finite volume method*. Pearson education, 2007.
[46] Miyazaki, T., and Y. Tominaga. "Wind tunnel experiment on flow field around a building model with a scale ratio of 4:4:1 placed within the surface boundary layer." In *Proceedings of Annual Meeting of Hokuriku Chapter, Architectural Institute of Japan*, pp. 201-204. 2003.
[47] Willemsen, Eddy, and Jacob A. Wisse. "Design for wind comfort in The Netherlands: Procedures, criteria and open research issues." *Journal of Wind Engineering and Industrial Aerodynamics* 95, no. 9-11 (2007): 1541-1550. https://doi.org/10.1016/j.jweia.2007.02.006
[48] Blocken, Bert, W. D. Janssen, and Twan van Hooff. "CFD simulation for pedestrian wind comfort and wind safety in urban areas: General decision framework and case study for the Eindhoven University campus." *Environmental Modelling & Software* 30 (2012): 15-34. https://doi.org/10.1016/j.envsoft.2011.11.009
[49] NEN. "NPR 6097:2006 Application of mean hourly wind speed statistics for the Netherlands." *Dutch Practice Guideline* (2006).
[50] NEN. "NEN 8100 Wind Comfort and Wind Danger in the Built Environment." *Netherlands Normalisation Institute, Dutch* (2006).
[51] Sanyal, Prasenjit, and Sujit Kumar Dalui. "Effects of courtyard and opening on a rectangular plan shaped tall building under wind load." *International Journal of Advanced Structural Engineering* 10, no. 2 (2018): 169-188. https://doi.org/10.1007/s40091-018-0190-4
[52] Barbano, Francesco, Silvana Di Sabatino, Rob Stoll, and Eric R. Pardyjak. "A numerical study of the impact of vegetation on mean and turbulence fields in a European-city neighbourhood." *Building and Environment* 186 (2020): 107293. https://doi.org/10.1016/j.buildenv.2020.107293
[53] Judd, M. J., M. R. Raupach, and J. J. Finnigan. "A wind tunnel study of turbulent flow around single and multiple windbreaks, part I: velocity fields." *Boundary-Layer Meteorology* 80, no. 1-2 (1996): 127-165. https://doi.org/10.1007/BF00119015

[54] Kementerian Air Tanah dan Sumber Asli. "Buku Panduan Penanaman Rhu." *Kementerian Air Tanah dan Sumber Asli*, 2022.
[55] Dong, Zhibao, Wanyin Luo, Guangqiang Qian, and Hongtao Wang. "A wind tunnel simulation of the mean velocity fields behind upright porous fences." *Agricultural and Forest Meteorology* 146, no. 1-2 (2007): 82-93. https://doi.org/10.1016/j.agrformet.2007.05.009
[56] Khodayari, Neda, Ahmad Hami, and Navid Farrokhi. "The effect of trees with irregular canopy on windbreak function in urban areas." *Iran University of Science & Technology* 31, no. 3 (2021): 1-12.
[57] Lee, Jin-Pyung, Eui-Jae Lee, and Sang-Joon Lee. "Shelter effect of a fir tree with different porosities." *Journal of Mechanical Science and Technology* 28 (2014): 565-572. https://doi.org/10.1007/s12206-013-1123-6
[58] Salim, Mohamed Hefny, K. Heinke Schlünzen, and David Grawe. "Including trees in the numerical simulations of the wind flow in urban areas: Should we care?." *Journal of Wind Engineering and Industrial Aerodynamics* 144 (2015): 84-95. https://doi.org/10.1016/j.jweia.2015.05.004
[59] Su, Junwei, Le Wang, Zhaolin Gu, Meimei Song, and Zhourong Cao. "Effects of real trees and their structure on pollutant dispersion and flow field in an idealized street canyon." *Atmospheric Pollution Research* 10, no. 6 (2019): 1699-1710. https://doi.org/10.1016/j.apr.2019.07.001
[60] Liu, Chenchen, Zhongquan Zheng, Hong Cheng, and Xueyong Zou. "Airflow around single and multiple plants." *Agricultural and Forest Meteorology* 252 (2018): 27-38. https://doi.org/10.1016/j.agrformet.2018.01.009
[61] Lyu, Junwei, Chien Ming Wang, and Matthew S. Mason. "Review of models for predicting wind characteristics behind windbreaks." *Journal of Wind Engineering and Industrial Aerodynamics* 199 (2020): 104117. https://doi.org/10.1016/j.jweia.2020.104117
[62] Liu, Benli, Jianjun Qu, Weimin Zhang, Lihai Tan, and Yanhong Gao. "Numerical evaluation of the scale problem on the wind flow of a windbreak." *Scientific Reports* 4, no. 1 (2014): 6619. https://doi.org/10.1038/srep06619
[63] Rosti, Marco E., Luca Brandt, and Alfredo Pinelli. "Turbulent channel flow over an anisotropic porous wall–drag increase and reduction." *Journal of Fluid Mechanics* 842 (2018): 381-394. https://doi.org/10.1017/jfm.2018.152
[64] Torshizi, Mohsen Rezaei, Abbas Miri, and Robin Davidson-Arnott. "Sheltering effect of a multiple-row Tamarix windbreak-a field study in Niatak, Iran." *Agricultural and Forest Meteorology* 287 (2020): 107937. https://doi.org/10.1016/j.agrformet.2020.107937
[65] Blocken, Bert, Peter Moonen, Theodore Stathopoulos, and Jan Carmeliet. "Numerical study on the existence of the venturi effect in passages between perpendicular buildings." *Journal of Engineering Mechanics* 134, no. 12 (2008): 1021-1028. https://doi.org/10.1061/(ASCE)0733-9399(2008)134:12(1021)
[66] Ma, Rui, Junran Li, Yanjun Ma, Lishan Shan, Xuelin Li, and Linyuan Wei. "A wind tunnel study of the airflow field and shelter efficiency of mixed windbreaks." *Aeolian Research* 41 (2019): 100544. https://doi.org/10.1016/j.aeolia.2019.100544
[67] Yinghua, Zhang, Kang Caizhou, Liu Shizeng, Tang Jinnian, Wei Linyuan, and Li Jinhui. "Windbreak effect of Picea mongolica farmland shelterbelt with different configuration." *Journal of Desert Research* 37, no. 5 (2017): 859.
[68] Lin, Xing Jun, Suzelle Barrington, Guangcai Gong, and Denis Choiniere. "Simulation of odour dispersion downwind from natural windbreaks using the computational fluid dynamics standard k-ε model." *Canadian Journal of Civil Engineering* 36, no. 5 (2009): 895-910. https://doi.org/10.1139/S08-057
[69] Okin, G. S., D. A. Gillette, and J. E. Herrick. "Multi-scale controls on and consequences of aeolian processes in landscape change in arid and semi-arid environments." *Journal of Arid Environments* 65, no. 2 (2006): 253-275. https://doi.org/10.1016/j.jaridenv.2005.06.029
[70] Burri, Katrin, Christof Gromke, Michael Lehning, and Frank Graf. "Aeolian sediment transport over vegetation canopies: A wind tunnel study with live plants." *Aeolian Research* 3, no. 2 (2011): 205-213. https://doi.org/10.1016/j.aeolia.2011.01.003
[71] Dupont, Sylvain, Gilles Bergametti, and Serge Simoëns. "Modeling aeolian erosion in presence of vegetation." *Journal of Geophysical Research: Earth Surface* 119, no. 2 (2014): 168-187. https://doi.org/10.1002/2013JF002875
[72] Bean, Allan, Robert W. Alperi, and C. A. Federer. "A method for categorizing shelterbelt porosity." *Agricultural Meteorology* 14, no. 1-2 (1974): 417-429. https://doi.org/10.1016/0002-1571(74)90035-1
[73] Fryrear, D. W., J. D. Bilbro, C. E. Yates, and E. G. Berry. "Modeling multirow wind barrier density." *Journal of Soil and Water Conservation* 55, no. 3 (2000): 385-392.